IEEE Access
Multidisciplinary | Rapid Review | Open Access Journal

Received August 23, 2018, accepted September 25, 2018, date of publication October 5, 2018, date of current version November 9, 2018.

Digital Object Identifier 10.1109/ACCESS.2018.2874131

Renewable Energy Assisted Cost Aware Sustainable Off-Grid Base Stations With Energy Cooperation

ABU JAHID[1], MD. KAMRUL HASAN MONJU[2], MD. EMRAN HOSSAIN[2], AND MD. FARHAD HOSSAIN[3], (Member, IEEE)

[1]Department of Electrical, Electronic and Communication Engineering, Military Institute of Science and Technology, Dhaka 1216, Bangladesh
[2]Department of Electrical and Electronic Engineering, Bangladesh University of Business and Technology, Dhaka 1216, Bangladesh
[3]Department of Electrical and Electronic Engineering, Bangladesh University of Engineering and Technology, Dhaka 1205, Bangladesh

Corresponding author: Abu Jahid (setujahid@gmail.com)

ABSTRACT With the growing awareness of environmental implications and fossil fuel crisis, renewable energy harvesting (EH) technology has shown remarkable aptitude in green cellular networking and is expected to be pervasively utilized by telecom operators aiming to reduce carbon footprints. To take the full advantage of renewable EH technology, we proposed an energy sustainable paradigm to address energy self-reliance, eco-sustainability, and minimize the networks energy cost while meeting the quality of service requirements. This paper investigates the techno-economic feasibility of integrated renewable energy powered off-grid cellular base stations (BSs) taking into the account of stochastic behavior of RE generation and traffic intensity for remote areas in Bangladesh. Thereafter, a hybrid energy cooperation framework is formulated to optimally determine the quantities of RE exchanged among BSs via physically installed power cables. Under the proposed framework, each BS is equipped with on-site solar module/wind turbine coupled with an independent storage device, whereas collocated BSs are inter-connected through resistive lines. Extensive simulation is carried out for evaluating optimal system architecture, energy yield analysis, and cost assessment in the context of downlink long-term evolution cellular networks varying different system parameters. Results demonstrate the effectiveness of the proposed system performance pertaining to net present cost and energy savings. Finally, a comprehensive comparison with other schemes is provided for further validation.

INDEX TERMS Energy cooperation, energy saving, sustainable cellular network, renewable energy, LTE.

I. INTRODUCTION

The number of mobile subscribers and their respective traffic volume has increased exponentially in the future due to the ubiquitous availability of internet access and affordable wireless devices to everyone. With the proliferation of wireless devices and applications, current Information and Communication Technology (ICT) network experiences high energy consumption occupies a leading position due to ever-increasing traffic demand [1]–[3]. It is estimated that the global mobile traffic is predicted to increase 69 exabytes per month by 2020 at an exponential multiplication rate of 45%. Consequently, the global annual electricity consumption for the telecommunication sector has increased from 219 TWh in 2007 to 354 TWh in 2012, which corresponds to an annual growth rate of 10%. This projection of energy consumption is expected to increase at an additional annual rate of 10% between 2013 and 2018. As the much expansion and up-gradation of cellular infrastructure across the globe, ICT sector could use as much as 51% of global electricity in 2030 if the necessary steps are not taken [4], [5]. Accordingly, telecom sectors have been implicated as the most energy-intensive consumer in ICT circle that is responsible for greenhouse gas (GHG) emissions and high operational expenditure (OPEX).

Currently, telecom sectors in ICT industry has been recognized as the main contributor to greenhouse gas emissions and leads 2.5-4% of total global carbon emissions [6], [7]. This increased energy consumption not only places an immense pressure on the electric grid but also exerts a detrimental effect on the economic aspects apart from the environmental implications. On the other hand, the pricing of the ICT services worldwide is decreasing gradually [8], leading to the heavy burden on cellular operators to curbing down energy consumption in order to maintain profitability. Therefore, energy efficiency (EE) is the key consideration for cellular operators with the purpose of reducing costs and emission-intensive carbon footprints while maintaining guaranteed quality of service (QoS) [9].

Uneconomical extension of commercial grid supply or the deployment of diesel generator (DG) to power up entire cellular networks has become less favorable due to the challenges related to reliability, high operational expenditure, and their adverse environmental aspects. Typically, a diesel generator (DG) is used to supply electricity remotely located BSs where the commercial grid is not present or not reliable. In addition, the concept of implementing DG to drive BS load has been recognized as less preferable owing to lower efficiency, routine operation and maintenance. Moreover, the conventional energy sources (coal, oil, natural gas, etc.) also leads to social problems such as global warming, acid rain, health hazardous, etc. [10]. All of these factors are continually growing over the upcoming years, and this uptrend issue is leading to a significant need for green cellular communications. With augmented consideration of both economic and environmental aspects, energy-efficient green cellular networking has drawn considerable attention in ICT sectors [11]. Green technology primarily focuses on the environmental, economic and energy concerns. The ultimate objectives of green communications are to enhance EE, minimize OPEX, eliminate greenhouse gas emissions, reduces dependency on external energy retailers and help to downward the pressure on energy prices.

Energy harvesting (EH) technology can be leveraged in the context of green wireless networking that can exploit renewable energy from readily available ambient sources such as solar, wind, biogas etc. Renewable energy resources are non-polluting, sustainable and cheap, are the key alternative to toxic-intensive fossil fuels in order to meet ever-increasing energy demand by ICT sectors worldwide [12], [13]. In the remotely located BS, transportation of non-renewable energy sources is quite challenging and expensive due to a transportation cost and rough terrain. As a result, locally available renewable energy is the most lucrative solution to power up BSs in isolated areas. However, a large extent of uncertainties is involved in designing a reliable renewable-based power generation system for remote areas due to the highly dynamic behavior of availability of sources. The mismatch between harvested energy and BS load variations may result in energy outage and service quality degradation.

In order to deal with such limitations, the BSs of the next generation cellular networks are provisioned to be powered by hybrid supplies has become a promising solution for enhancing efficient networks operations. Integrated use of different renewable energy resources reinforces the reliability and quality of services (QoS) for envisaged green cellular networks with the reduction of system cost. Depending on the site conditions, aggregated technology such as PV/Wind is a viable solution of the growing energy crisis and the scarcity of commercial grid supply. The space constraints of on-site RE energy harvesting (i.e., installation of sufficient solar panels, wind turbines) is the key limiting factor of sufficient renewable energy generation.

Recently, energy efficiency (EE) performance of cellular networks has been widely studied adopting the energy sharing technique among multiple collocated BSs via smart grid or any external physical power lines [1], [14], [15]. To facilitate energy transfer over the installed resistive power lines have some practical constraints and economically unviable for large-scale cellular networks. This approach is not feasible for long-haul communication link due to higher installation cost, large resistive power losses and a right way of restriction, etc. Physical cabling connection may be plausible for energy sharing among BSs within small zones. For long-haul communication, smart grid infrastructure is an emerging option for energy sharing instead of installing external physical lines. Moreover, necessary care and an extensive assessment of energy requirements must be taken during installation as physical power lines are permanent. Nevertheless, energy cooperation is beneficial when the locally available RE generation is high enough to meet its own energy demand; it would then share surplus energy from its storage with the requesting BS. However, the terms energy sharing and energy cooperation are interchangeable throughout this paper.

The rest of the paper is organized as follows. A through review of related works is discussed in section II. Section III presents the detailed discussion of system model along with solar energy model, energy storage device, wind generation, and DG power system. A load dependent BS power model, mathematical model of power reliability and energy cooperation mechanism are also presented in the same section. Cost modeling and optimization problem are outlined in the section IV and section V respectively. Simulation setup and performance analysis with an insightful discussion are demonstrated in section VI. Finally, this paper is concluded in section VII.

II. RELATED WORKS

This section attempts to discuss the current status of the conducted researches in the field of optimal sizing and installing of integrated renewable energy assisted hybrid power cellular system. Recently, eco-sustainability has received considerable attention due to the dramatic surge of energy demand and limited fossile fuel resources. Being inspired for cutting down the energy cost and up trending concern of global climate change, green cellular communication has drawn widespread attention especially in remote off-grid areas. Currently, several research works are conducted focusing on the deployment of renewable energy such as solar PV panels to increase self-reliance and eco-sustainability of RAN infrastructure [12], [16], [17]. Chamola and Sikdar [12] present an overview of the novel design and deployment of solar powered cellular base stations. The article also discusses current challenges in the implementation and operation of such base stations along with some of the critical solution. Zhang *et al.* [16] proposed a heuristic algorithm for the identification of the minimum cost solution of solar PV assisted LTE macrocell base station. A comprehensive study has been carried out to address the sustainability of an autonomous solar power system for heterogeneous cellular networks based on the characteristics of solar radiation exposure in South Korea [17]. Gong *et al.* [18] formulated the substantial enhancement of EE as well as minimization of the average on-grid consumption combining both BS sleep mode approach and renewable energy supply, which do not require hardware upgrade. However, this article does not account both the traffic intensity and solar generation diversity. Despite the potential advantages of using RE sources, several challenges such as energy are lost in converter during energy conversion process and also in the battery bank, load transients and environmental disasters are still existed that affect system stability.

Hybrid energy supply (i.e., aggregate technology) has emerged as a long-term solution and feasible option for sustainable energy supply in LTE base stations [19], [20]. Alsharif and Kim [19] examined the feasibility of hybrid solar PV/WT solution to feed the remote LTE BSs aiming to minimize the operational expenditure (OPEX). Nevertheless, this study does not consider realistic traffic arrival intensity to be served by BS. A hybrid powered green multi-cell cooperation for heterogeneous networks is investigated in [20]. The authors suggest a greedy algorithm based on tempo-spatial characteristics in order to cut down conventional grid energy. Jahid and Hossain [21] analyzed the feasibility of hybrid PV/DG/Battery power supply option for macro BSs aiming to maximize the green energy utilization. Several key aspects including optimal system design, energy-cost analysis, and carbon footprints have been thoroughly studied for evaluating EE for the considered homogeneous networks.

The concept of energy sharing among BSs via smart grid (SG) or external physical resistive power lines has emerged in the literature of [1], [14], and [22]. The realization of efficient energy sharing mechanism among BSs in smart grid (SG) powered cellular networks based on the level of a priori knowledge of the system about RE generation has been analyzed in [1]. An optimized energy exchange framework between two BSs that are physically connected is presented in [14]. On the other hand, a framework for energy sharing among three macro cells using external physical power lines is proposed in [22]. It is worth mentioning that energy cooperation is feasible when the on-site RE generation is high enough to meet its own energy demand, and BS would never sacrifice its own performance while sharing green energy among them.

BSs in radio access networks (RAN) are dimensioned for peak hour data traffic; thus, the energy utilization of BSs can be very inefficient during low-traffic or off-traffic hours. Adjusting the transmission power of the transceivers according to traffic arrival intensity is the most intuitive idea to optimizing power saving for the considered cellular networks. Switching off some redundant BSs during off-peak hours is an alternative way to improve EE, but sleep-mode based algorithm is not efficient when the traffic load is intensive. This paper deals with the energy management of hybrid power LTE cellular networks including techno-economic optimization, sustainability, long-term reliability, and key challenges particularly Patenga shore areas in Bangladesh. In Patenga zone, BSs experiences good sunlight and windy conditions, RE sources offer an excellent alternative to conventional supply in a most economical and energy-efficient way. A traffic aware modeling method has been made to estimate the potential of locally available renewable energy resources and energy demands of the study area accounting energy sharing mechanism to make the networks more realistic.

MOTIVATIONS & CONTRIBUTIONS

Optimum unit sizing of renewable energy sources, battery bank and power electronic converter is essential for cost-efficient utilization in the proposed cellular system. Over sizing the system components will enhance the output power as well as system cost. The optimal design ensures the lowest net present cost with high reliability of system operation. Based on the literature review carried out and aforementioned identified research gaps, this paper explores the techno-economic feasibility of hybrid solar-wind-battery based integrated renewable system to powering remote LTE cellular BSs in Bangladesh. Particularly, we emphasize the green energy cooperation framework via intelligently installed physical connections among surrounded BSs. Recently, the next generation cellular networks are widely deployed Radio Remote Head (RRH) unit to the conventional macrocell. RRH replaces the coaxial cable by a fiber optic link connected between baseband unit and power amplifier sections. Macro BS with RRH has the inherent potential to reduce feeder cable loss. In addition, no cooling arrangement is needed and hence, minimize the overall energy consumption. LTE BS with RRH offers a high level of flexibility in cell site construction and increase system efficiency without sacrificing QoS [27]. Moreover, different combinations of power supplies option have been compared for the intended wireless system using Hybrid Optimization Model for Electric Renewable (HOMER) software. Afterwards, a suitable combination for the study area is recommended in light of economic, technical and social aspect. The principal contributions of this paper are summarized as follows:

- This paper proposes real-time traffic steering framework for the modern cellular networks by deploying hybrid renewable power supply for distant BSs. We then explore the optimal system architecture and techno-economic criteria of hybrid PV/WT system to feed off-grid macro BSs using HOMER.
- The benefit of radio remote head (RRH) unit integration to the conventional macrocell varying different system

parameters are thoroughly examined in consideration of traffic and RE generation dynamics.

- A technique of energy sharing framework is developed among collocated BSs for maximizing the green energy utilization based on the surplus electricity generation. Henceforth, we thoroughly investigate average energy savings with the incorporation of inter-BS energy cooperation policy.
- Extensive simulations are carried out to analyze the system performance in terms of energy yield, cost analysis, and greenhouse gas emissions effects over the considered project duration varying transmission power, system bandwidth, solar radiation exposure etc., which has not been investigated yet in literature. To the end, sustainability of the proposed system has been critically analyzed over the project duration.

III. SYSTEM MODEL

A hybrid power system integrates different energy sources to mitigate the weakness of RE sources to attain reliable energy supply in telecom BSs. This section presents the proposed system model along with renewable energy generation model, BS power consumption model, and energy sharing algorithm in the context of off-grid LTE cellular networks. Symbols and notations used in the following sections are summarized in Table 1.

A. NETWORK LAYOUT

A downlink LTE homogeneous cellular network comprising a set of N collocated BSs $\mathbb{B} = \{\mathcal{B}_1, \mathcal{B}_2, \ldots.., \mathcal{B}_N\}$ and covering an area $\mathcal{A} = \{\mathcal{A}_1 \cup \mathcal{A}_2 \cup \ldots \cup \mathcal{A}_N\} \subset \mathbb{R}^2$ is considered. Here, $\mathcal{A}_i$ is the coverage area of BS $\mathcal{B}_i$, $\forall i \epsilon \{1, \ldots, N\}$. All the macro BSs are incorporated with tri-sector 2/2/2 antennas in a hexagonal grid layout. We consider a finite-horizon time-slotted system with slot index n, $1 \leq n \leq T$, and T denotes the total number of time slots. We consider all the macro BSs are powered by hybrid supplies including a combination of different renewable energy resources. In such cellular networks, each BS is equipped with independent on-site solar energy harvester, wind turbine (WT), converter, and sufficient energy storage device such as batteries with a smart energy management unit (EMU). An EMU is used to protect battery life through preventing overcharging and restricts deep discharging of the battery bank and also enables the integration of multiple energy sources. In addition, the neighboring BSs in the first tier are assumed to be connected with each other through physical resistive power line for energy sharing. A segment of homogeneous network with seven macro sites architecture is shown in Fig. 1. The proposed network layout presents the two subsystems including the hybrid power supply and the BS load. We contemplate that the cellular network experiences variable traffic throughout the day and user equipments (UEs) are assumed to be randomly distributed over the geographical area. The nomenclature 2/2/2 represents each macrocell has six transceivers i.e. three sectors with 2 antennas per sector.

TABLE 1. Summary of the notations and symbols.

$AES(i,t)$	Average energy savings of i^{th} BS at time t
$\mathcal{BW}$	Bandwidth (MHz)
B_{aut}	Battery bank autonomy (hour)
B_{DoD}	Battery depth of discharge
B_{life}	Battery lifetime (year)
B_{loss}	Energy lost in battery bank (kWh)
B_{SoC}	Battery state of charge
C_{PV}	Capacity of solar PV arrray (kW)
C_{loss}	Loss due to energy conversion (kWh)
E_{batt}	Battery bank storage capacity (kWh)
E_{BS}	BS energy consumption (kWh)
E_{DG}	DG energy production (kWh)
E_{gen}	Total generated energy (kWh)
E_{PV}	Energy generated from solar PV array (kWh)
E_{share}	Shared electricity (kWh)
E_{sur}	Excess electricity (kWh)
E_{WT}	Energy production from wind turbine (kWh)
$\mathcal{E}^i$	Total collected energy of $\mathcal{B}^i$ from surrounded BSs
f_{PV}	PV derating factor
F_c	Diesel consumption (L)
$LCOE$	Levelized cost of electricity ($/kWh)
M	Number of neighboring BSs
N	Total number of BSs
N_{batt}	Number of battery cells
N_{PV}	Number of PV modules
N_{TRX}	Number of transceiver
P_{BB}	Power consumption of baseband unit (W)
P_{RF}	Power consumption of radio frequency unit (W)
P_{nom}	Nominal power of solar module (W)
P_{TX}	BS transmit power (W)
Q_{nom}	Nominal capacity of single battery cell (Ah)
Q_{tp}	Annual battery throughput (kWh)
S^i	Energy storage at battery bank of i^{th} BS $\mathcal{B}^i$
V_{nom}	Nominal voltage of each battery cell (V)
χ	BS traffic load
δ	Dual axis sun tracking factor
γ_d	Daily solar radiation ($kWh/m^2/day$)

B. SOLAR PV SYSTEM

Energy harvesting for wireless communications mainly derives from an ambient energy sources, e.g., solar, wind etc. The daily solar energy generation shows temporal dynamics over a period of a day in the given area and exhibits spatial dynamics with geographical location. For example, average annual solar energy generation profile for Patanga city in Bangladesh is depicted in Fig. 2. Fig. 2 presents the temporal variation of solar energy generation for 1 kW PV module capacity is estimated using System Advisory Model (SAM) [23].

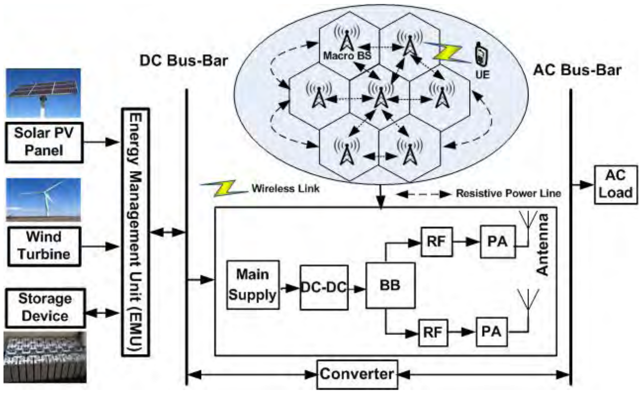

FIGURE 1. A section of the proposed network architecture with hybrid energy supply.

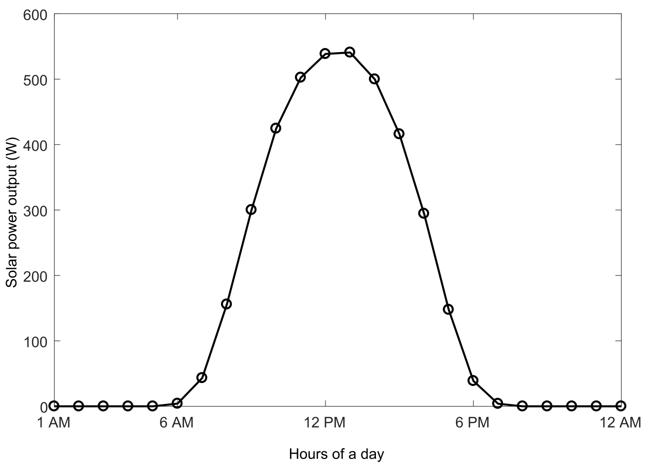

FIGURE 2. Average hourly solar energy generation in a day.

The RE generated at $\mathcal{B}^i$, $i \in \{1, \ldots, N\}$ during time slot n is modeled as a random variable denoted by $r_i\ (t) \in [0, r_i{}^{max}]$, where $r_i{}^{max}$ is maximum available solar energy generation by $\mathcal{B}^i$. The green power generation can be defined as $\int_{(n-1)\tau}^{n\tau} b_i(t)dt = r_i(t)$, where $b_i(t)$ is obtained from the instantaneous solar power profile as depict in Fig. 2 and τ is the duration of each time slot. Hence, this energy quantities represent the temporal averages over the corresponding time slots. The time varying average solar energy generation, $\bar{r}_i(t)$ is characterized by the following model [1]

$$\bar{r}_i(t) = \frac{r_i{}^{max} exp^{-(n-\beta_i)^2}}{\delta_i^2} \tau \tag{1}$$

In this model, β_i represents the position in time of the peak generation chosen to be noon, i.e. 12 hours, $\forall i \in \{1, \ldots, N\}$, δ_i indicates the shape width at half maximum of the peak, chosen to be 3 hours, $\forall i \in \{1, \ldots, N\}$, and the time duration of each slot τ is one hour.

The amount of solar energy generation is heavily depends on the geographic location, beam radiation, panel materials, environmental implications and tracking mode. Total amount of energy generated from the solar PV array can be calculated using HOMER [19]

$$E_{PV} = C_{PV} \times \gamma_d \times f_{PV} \times \delta \tag{2}$$

where C_{PV} is the rated capacity of the solar PV array in kW, γ_d is the daily solar radiation in $kWh/m^2/day$, f_{PV} derating factor and δ represents the dual-axis sun tracking mode factor. Dust, wire loss, temperature etc. can also affect output solar power.

The number of PV modules (N_{PV}) required to generate a given peak power (P_p) can be expressed as

$$N_{PV} = \frac{P_p}{P_{nom}} \tag{3}$$

where P_{nom} is the nominal power of solar module. The parameters of solar module used in the simulation are summarized in the Table 2. For instance, 1 kW peak power solar array requires 4 independent Sharp solar modules according to Table 2.

TABLE 2. Solar panel parameters.

Parameters	Type (Value)
Solar module type	Sharp ND-250QC (poly crystalline)
Nominal voltage (V)	29.80 V_{DC}
Nominal current (A)	8.40 Amp
Maximum power (P_{max})	250 $Watt$
Open circuit voltage (V_{oc})	38.3 V_{DC}
Short circuit current (I_{sc})	8.90 Amp
Tracking mode	Dual axis

HOMER calculates the average radiation from the global horizontal irradiance (GHI) by entering GPS coordinates in the particular area. The clearness index defines the solar radiation is transmitted to the surface of the earth and measures the clearness of the atmosphere. Clearness index (CI) is heavily depends on the solar radiation intensity in a month whose value varies in range between 0 to 1.

HOMER calculates the intensity of solar radiation (γ_d) at the top of the earth atmosphere using following equation [24]

$$\gamma_d = \gamma_c(1 + 0.033cos\frac{360n}{365}) \tag{4}$$

where n is the number of days in a year and I_c is the solar constant $= 1.367\ kW/m^2$. Fig. 3 demonstrates the average solar resource profile for one year period in Bangladesh. The annual solar irradiation profile with CI for Bangladesh is shown in Fig. 3.

C. WIND ENERGY SYSTEM

Due to the random nature of solar energy generation, the available solar energy may not guarantee the quality of service (QoS) for a BS to run for a whole day. Wind turbine is integrated with PV array in order to ensure reliable network operations. Wind energy generation depends on site location, weather system and height above the ground. WT converts

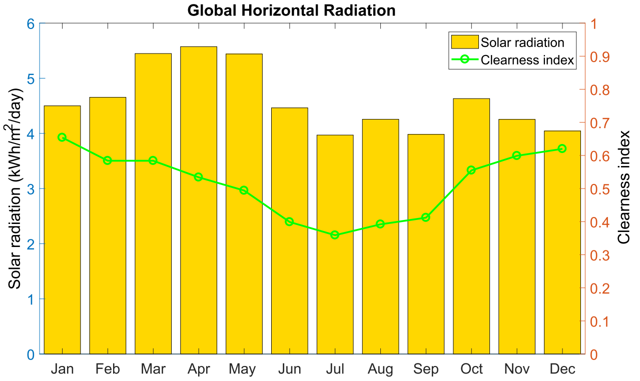

FIGURE 3. Average annual profile of solar radiation.

the flowing wind speed into mechanical energy and then into electricity. Weibull probability density function of wind speed (v) is defined as [25]

$$f(v,k,c) = (\frac{k}{c})(\frac{v}{c})^{k-1} exp[-(\frac{v}{c})^k] \tag{5}$$

where c is the scale parameter, k is the shape parameter and $v \geq 0, k > 1, c > 0$.

The output power of WT (P_{WT}) is heavily depends on its rated power (P_r), rated speed (v_r), cut-in speed (v_{ci}), and cut-out speed (v_{co}). The mathematical model of P_{WT} can be presented as [25]

$$P_{WT} = \begin{cases} 0, & for\ 0 \leq v < v_{ci}\ and\ v > v_{co} \\ av^3 + bP_r, & for\ v_{ci} \leq v < v_r \\ P_r, & for\ v_r \leq v \leq v_{co} \end{cases} \tag{6}$$

Constants a and b are function of rated speed and cut-in speed, can be expressed as follows

$$a = \frac{P_r}{{v_r}^3 - {v_{ci}}^3}$$
$$b = \frac{{v_{ci}}^3}{{v_r}^3 - {v_{ci}}^3}$$

Hourly energy production from a WT at a given site can be calculated as

$$E_{WT} = \sum_{v=0}^{v_{co}} P_{WT} \times f(v,k,c) \tag{7}$$

The approximate power contained in the wind kinetic energy is expressed by [19]

$$P_{WT} = \frac{1}{2}\rho v^3 C_p \tag{8}$$

where C_p is the coefficient of the Betz limit, which can achieve a maximum value of 59% for all types of wind turbines and ρ is the monthly air density (kg/m^3). HOMER assumes a standard air density of 1.225 kg/m^3, which corresponds to standard temperature and pressure conditions. The parameters of Whisper200 wind turbine model is presented in Table 3 and its power output curve is depicted in Fig. 4.

TABLE 3. Wind Turbine parameters.

Parameters	Type (Value)
Model	Whisper 200
Rated output (P_r)	1 kW
Cut-in speed (v_{ci})	3.1 m/s
Rated speed (v_r)	11.6 m/s
Cut-in speed (v_{co})	24 m/s
Rotor diameter	2.72 m
Swept area	5.8 m^2

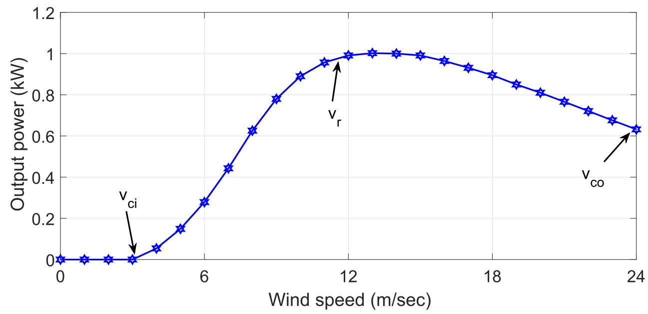

FIGURE 4. Power output for Whisper200 WT.

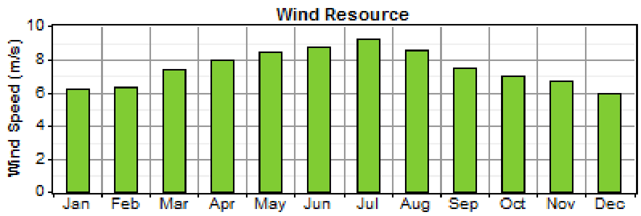

FIGURE 5. Monthly average wind speed for Patanga in Bangladesh [26].

The monthly average wind speed for Patanga in Bangladesh is shown in Fig. 5. In the rainy season (e.g. June & July month), the wind speed is found considerably higher compared to other seasons. The high power wind generation is compensated by the lesser solar power output during rainy season leading to minimize the fluctuation of combined RE production. However, the annual average wind speed is 7.48 m/s as measured from Fig. 5.

D. DIESEL GENERATOR

Diesel generator (DG) can be integrated along with RE sources in where green energy is not sufficient to fulfill the BS demand or to mitigate the fluctuations of RE generation. In this paper, LTE wireless networks entirely operated by integrated PV/WT green energy sources without any provision of DG concept. In the result section, the proposed framework is compared with DG enabled hybrid power system for validation of the system effectiveness. We present DG power system model to realize energy generation, cost-efficiency and carbon emission analysis. Hourly energy produced by a DG (E_{DG}) with the given rated power output (P_{DG}) can be expressed as

$$E_{DG} = P_{DG} \times \eta_{DG} \times t_{op} \quad (9)$$

where η_{DG} is the efficiency of DG set and t_{op} operational running hours. The DG size (P_{DG} in kW) can be calculated as

$$P_{DG} = \frac{BS\ load\ in\ kW}{\eta_{DG} \times \eta_C} \quad (10)$$

where η_C means the converter efficiency. The diesel consumption (in L) is calculated as follows

$$F_c = E_{DG} \times f_{sp} \quad (11)$$

where f_{sp} is the specific fuel consumption. Generally, a DG set emit carbon footprints of 2.68 kg/L [21].

E. CONVERTER

A converter is required for systems in which AC components serve DC load or vice-versa. An inverter convert a low DC voltage into a usable 220V AC voltage with the desired frequency of the load. On the other hand, rectifier convert electrical energy from the AC to DC form with the compatible bus voltage. In this study, dual mode operation of the converter is implemented to supply both DC load and AC load.

F. ENERGY STORAGE MODEL

Energy storage systems (ESS) such as batteries plays a significant role to offset the unpredictable variation of the RE generation. ESS store excess electricity for future consumption during night, load-shedding, or if renewable energy is failed to feed the BS demand. Rechargeable batteries are modular and non-pollutant device that store electrical energy in the form of chemical energy which is not immediately used to run BS. A battery bank (BB) is a backup device and commonly used in communication systems to ensure 100% energy reliability. Various types of battery storage applications include lead acid, nickel cadmium, sodium sulphur, vanadium redox batteries etc. Without losing the generality, Trojon L16P battery model is widely used in cellular BSs due to their large capacity, low cost, high reliability, low self-discharging, and requires low maintenance. The characteristic nominal capacity of Trojon L16P battery is depicted in Fig. 6.

Battery state of charge (B_{SoC}) defines the battery charging-discharging state that is usually measured in percentage. For example, $B_{SoC} = 0\%$ means the battery is full empty. The maximum SoC ($B_{SoC\,max}$) defines the nominal capacity of the battery bank. On the other hand, the minimum SoC ($B_{SoC\,min}$) is the lower threshold limit of battery discharge. The depth of discharge (B_{DoD}) is the maximum energy supplied by the battery bank and is computed as [21]

$$B_{DoD} = (1 - \frac{B_{SoC\,min}}{100}) \quad (12)$$

Battery bank stores excess electricity when the total power generation is greater than the hourly BS energy demand.

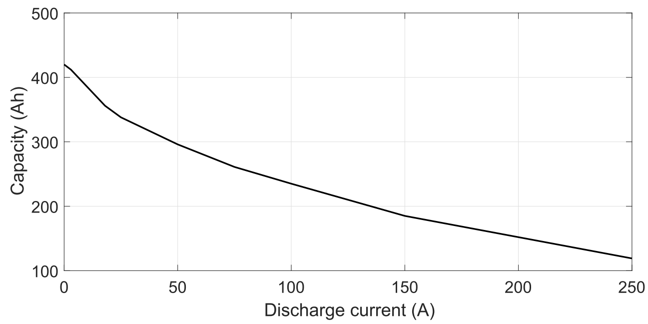

FIGURE 6. Characteristics of Trojon L16P battery capacity with discharging current.

The available battery bank capacity at every hour τ can be estimated as follows

$$E_{batt}(\tau) = E_{batt}(\tau - 1) + E_{DC}(\tau) \times \mu - E_{BS}(\tau) \quad (13)$$

$$E_{DC}(\tau) = E_{PV} + E_{WT} \quad (14)$$

where $E_{batt}(\tau - 1)$ is the energy storage capacity in batteries in previous state, $E_{DC}(\tau)$ is the energy harvested from DC power sources such as solar PV array and wind turbine. μ is the charging efficiency of battery i.e., the percentage of storage energy retained after unit period of time. For example, $\mu = 0.9$ indicates that 10% energy will be lost in the storage during the time interval. $E_{BS}(\tau)$ represents the hourly energy demand by the cellular BS.

The maximum and minimum battery bank storage capacity in kWh can be determined as follows

$$E_{battmax} = \frac{N_{batt} \times V_{nom} \times Q_{nom}}{1000} \times B_{SoC\,max} \quad (15)$$

$$E_{battmin} = \frac{N_{batt} \times V_{nom} \times Q_{nom}}{1000} \times B_{SoC\,min} \quad (16)$$

where N_{batt} is the number of battery cells in the battery bank, V_{nom} is the nominal voltage of each battery cell (V) and Q_{nom} is the nominal capacity of single battery in Ah.

Battery bank autonomy (B_{aut}) plays a vital role during the absence of power supply sources. B_{aut} represents the potential number of days that the battery bank drive the BS load independently. This parameter can defined as the ratio of battery bank size to the BS load; as expressed by the following equation

$$B_{aut} = \frac{N_{batt} \times V_{nom} \times Q_{nom} \times B_{DoD} \times (24h/day)}{L_{BS}} \quad (17)$$

where L_{BS} average daily BS load in kWh. Battery bank backup counterbalances the mismatch between RE generation and BS energy demand during energy deficiency.

On the other hand, battery lifetime (B_{life}) is an another important factor which is directly related to the total replacement cost during the given project lifecycle. HOMER calculates the battery lifecycle based on the following equation [19]

$$B_{life} = min(\frac{N_{batt} \times Q_{life}}{Q_{tp}}, B_f) \quad (18)$$

where Q_{life} is the lifetime throughput of a single battery (kWh), Q_{tp} is the annual battery throughput in kWh and B_f is the battery float life in years.

TABLE 4. Macro BS power consumption at maximum load of a LTE system for 10 MHz bandwidth [27].

Components	Parameters	w/o RRH	with RRH
BS	Type	Macro	Macro
	P_{TX} [W]	20	20
	Feeder loss σ_{feed} [dB]	3	0
PA	Back-off [dB]	8	8
	Max PA out [dBm]	54	51
	PA efficiency η_{PA} [%]	31.1	31.1
	Total PA, $\frac{P_{TX}}{\eta_{PA}(1-\sigma_{feed})}$ [W]	128.2	64.4
RF	P_{TX} [W]	6.8	6.8
	P_{RX} [W]	6.1	6.1
	Total RF, P'_{RF} [W]	12.9	12.9
Baseband, BB	Radio (inner Tx/Rx) [W]	10.8	10.8
	Turbo code(outer Tx/Rx) [W]	8.8	8.8
	Processors [W]	10	10
	Total BB, P'_{BB} [W]	29.6	29.6
DC-DC	σ_{DC} [%]	7.5	7.5
Cooling	σ_{cool} [%]	10	0
Mains Supply	σ_{MS} [%]	9	9
Sectors		3	3
Antennas		2	2
Total power [W]		**1350**	**754.8**

Throughput defines the state of energy level of the battery bank. In other words, the annual energy storage throughput is the amount of energy that cycles through the battery bank in a year. Battery bank lifetime decreases either from use or from aging effect. On the other hand, battery float life implies the length of the time that storage system will last before replacement.

The size of battery bank depends on the BS power consumption and the duration that support load demand autonomously. Indeed, the longer the battery backup means the larger storage capacity which leads to high cost. Additionally, a larger battery bank would take a longer time to take charge and thus, it is a crucial issue to figure out optimal battery sizing. The number of batteries in series is equal to the DC bus-bar voltage (V_{bb}) divided by the nominal voltage rating (V_{nom}) of the selected battery model.

$$N_{batt}^{series} = \frac{V_{bb}}{V_{nom}} \tag{19}$$

For instance, 8 batteries will be interconnected in series if the BS load operated at 48V DC bus bar of LTE BS for 6 V nominal voltage. The number of parallel paths is found by dividing the total number of batteries by N_{batt}^{series}.

G. BS POWER CONSUMPTION MODEL

The power consumption of a typical BS varies directly to their respective traffic load demand. Generally, traffic demand at individual BS are highly dynamic over time and space and hence, mobile traffic volume exhibits tempo-spatial diversity.

Table 4 summarizes the power consumption of each individual elements of LTE macro BS. The total BS power consumption for two different configurations presented in Table 4 is shown for peak traffic load. Cellular networks are widely designed to serve UEs on peak-time periods results in a significant wastage of electrical energy during off-peak time. The BS activity could be adapted according to the real traffic load that can inherently avoid the waste of energy due to peak dimensioning. It is important to evaluate energy consumption of the typical BS considering incoming traffic arrivals in order to dimensioning the proposed hybrid power system. However, the BSs energy consumption can be sub-divided into two parts: the static energy consumption and the dynamic energy consumption. An approximate traffic pattern is shown in Fig. 7 can be estimated by using Poisson distribution model as follows

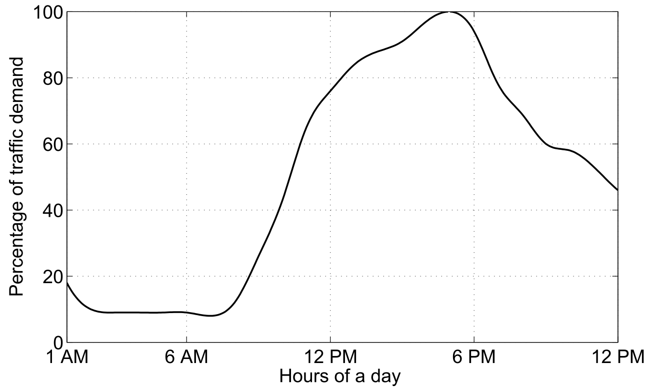

FIGURE 7. Daily traffic load profile.

$$\lambda(t) = \frac{p(t,\alpha)}{max[p(t,\alpha)]} \tag{20}$$

$$p(t,\alpha) = \frac{\alpha^t}{t!}e^{-\alpha} \tag{21}$$

where $\lambda(t)$ is the normalized traffic distribution, $p(t,\alpha)$ is the Poisson distribution function of traffic demand at a particular period of time, and α is the mean value where peak number of traffic arrivals occur at 5 PM.

The total approximate power consumption considering number of transceivers (N_{TRX}) and actual traffic intensity (χ) is defined as [27]

$$P_{in} = \begin{cases} N_{TRX}[P_1 + \triangle_p P_{TX}(\chi - 1)], & \text{if } 0 < \chi \leq 1 \\ N_{TRX}P_{slp}, & \text{if } \chi = 0 \end{cases} \tag{22}$$

where $P_1 = P_0 + \triangle_p P_{TX}$ is the the maximum power consumption of a BS sector and P_0 is the consumption at idle state. The load dependency is accounted for by the power gradient, $\triangle_p$. The scaling parameter $\chi = 1$ indicates that a fully loaded system and and $\chi = 0$ indicates idle state. Furthermore, a BS without any traffic load enters into sleep mode with lowered consumption, P_{slp}. The dynamic power consumption is varied with traffic loading parameter χ as seen from Fig. 8 for 10 MHz bandwidth. The parameters of BS load are summarized in Table 5.

TABLE 5. BS approximate power consumption model parameters [27].

BS Type	N_{TRX}	$P_{TX}[W]$	$P_0[W]$	$\triangle_P$	$P_{slp}[W]$
Macro w/o RRH	6	20	130	4.7	75
Macro with RRH	6	20	84	2.8	56

Now P_1 can be expressed as below [28]

$$P_1 = \frac{P_{BB} + P_{RF} + P_{PA}}{(1-\sigma_{DC})(1-\sigma_{MS})(1-\sigma_{cool})} \tag{23}$$

where P'_{BB} and P'_{RF} are the power consumption of based-band unit and radio frequency transceiver respectively. Losses incurred by DC-DC power supply, mains supply and active cooling can be approximated by the loss factors σ_{DC}, σ_{MS} and σ_{cool} respectively. However, power consumption in the power amplifiers is represented by P_{PA} which depends on the maximum transmission power and power amplifier efficiency η_{PA} and can be given as follows

$$P_{PA} = \frac{P_{TX}}{\eta_{PA}(1-\sigma_{feed})} \tag{24}$$

However, both the power consumption P_{BB} and P_{RF} scale linearly with bandwidth $\mathcal{BW}$ and the number of transceiver chain (N_{TRX}) while the other parameter remains unchanged following in (23). The formulation of power consumption scaling with the transmission bandwidth $\mathcal{BW}$ can be evaluated as [28]

$$P_{BB} = N_{TRX}\frac{\mathcal{BW}}{10\ MHz}P'_{BB} \tag{25}$$

$$P_{RF} = N_{TRX}\frac{\mathcal{BW}}{10MHz}P'_{RF} \tag{26}$$

The power consumption of the air-conditioning unit depends on the internal temperature of the BS cabinet and approximately consumes 10% of total power consumption in the macrocell without RRH [27]. On the other hand, no cooling equipment is required for macrocell with RRH configuration as observed from Table 4. We assume that air conditioner run 18 hours in a day with 6 hours running and 2 hours shut off, and so on. For example, aircon unit consumes 135 watt per hour for 10 MHz bandwidth and hence, the annual energy consumption of cooling unit is 887 kWh under macro BS without RRH system. Also, an auxiliary 25 W lamp as an AC load is connected to BS running from 7 PM to 6 AM. As a result, the energy consumption by 25W lamp is 109.5 kWh/year for 12 hours running period in a day. The total annual energy consumption of two different model LTE BS is listed in Table 6 for different bandwidth. Consequently, the percentage of DC load and AC load sharing of total consumption is 91.7% and 8.3% respectively for 10 MHz bandwidth under macrocell without RRH scheme. Fig. 9 and Fig. 10 represents the seasonal AC load profile for macro BS with RRH and macrocell without RRH respectively in HOMER platform. The empty region (dark shade in DMap) in Fig. 9 between 6 AM to 6 PM implies the zero ac load consumption.

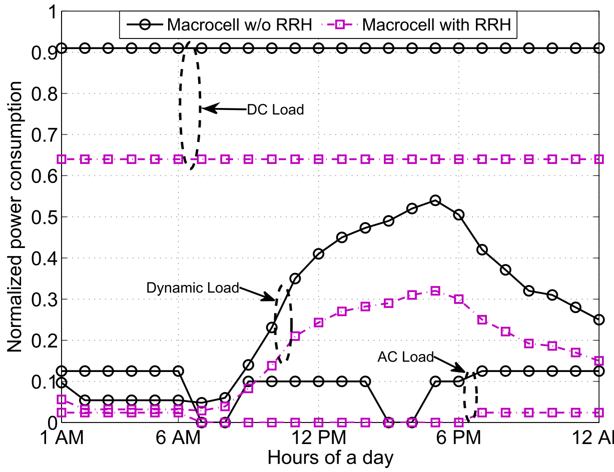

FIGURE 8. Hourly normalized load profile for macrocell under actual traffic demand for $\mathcal{BW}$ = 10 MHz and P_{TX} = 20W.

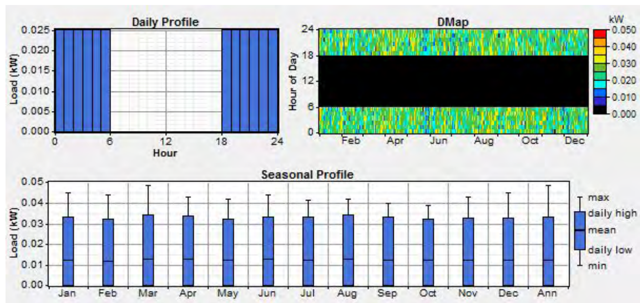

FIGURE 9. Seasonal AC load profile of macro BS with RRH for $\mathcal{BW}$ = 10 MHz and P_{TX} = 20W in HOMER platform.

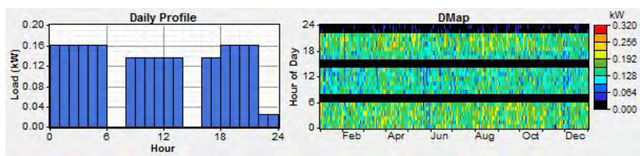

FIGURE 10. Seasonal AC load profile of macro BS without RRH for $\mathcal{BW}$ = 10 MHz and P_{TX} = 20W in HOMER platform.

TABLE 6. Annual energy consumption (kWh/yr).

$\mathcal{BW}$ (MHz)	Macro w/o RRH		Macro with RRH	
	P_{TX}=20W	P_{TX}=40W	P_{TX}=20W	P_{TX}=40W
5	10463	19372	6048	10463
10	11952	20844	7520	11935
15	13426	22321	9000	13406
20	14895	23793	10474	14878

With the integration of RRH with conventional macrocell substantially reduce annual energy consumption while maintaining desired quality of service (QoS) as clearly evident from Table 6. However, LTE cellular BS typically operates at 20W (43 dBm) and 40W (46 dBm), but 20 W power is also commonly used in many research articles in the context of cellular communications [28]. With the increment of BS transmission power (P_{TX}), for instance to 40W (i.e., 46 dBm), received signal power will certainly increase, while total energy consumption will also rise simultaneously. Under 10 MHz transmission bandwidth, macro BS with RRH can achieve 37.3% and 42.74% energy savings over conventional macrocell configuration (i.e., macro BS with no RRH) for 20W and 40W transmit power respectively. It can be safely inferred that macrocell without RRH configuration has need of higher installed capacity of renewable equipments for the same traffic demand which may elevate NPC of the entire system. Therefore, the results presented in this paper are analyzed for the proposed macrocell with RRH scheme with hybrid power supplies.

H. POWER RELIABILITY

The annual capacity shortage (R_{CS}) is identified as a power reliability term in this study. It can be defined as the ratio of annual energy deficiency (E_{CS}) to the annual BS load demand (E_{BS}).

$$R_{CS} = \frac{E_{CS}}{E_{BS}} \tag{27}$$

where the values of E_{BS} in kWh/yr are presented in Table 6. In this paper, we simulate the proposed system for zero E_{CS} and can be formulated as follows

$$E_{CS} = E_{BS} - E_{gen} \tag{28}$$

where E_{gen} is the generated electricity in kWh/yr and can be written as

$$E_{gen} = E_{PV} + E_{WT} \tag{29}$$

System reliability can be assured when generated energy meets the BS load demand for the considered project lifetime.

I. SURPLUS ELECTRICITY

For the proposed hybrid power cellular system, excess electricity is generated under the condition when total energy generation go beyond the BS load demand and can be computed as follows

$$E_{sur} = E_{gen} - E_{BS} - C_{loss} - B_{loss} \tag{30}$$

where C_{loss} and B_{loss} represents the annual converter loss and battery loss respectively.

J. ENERGY COOPERATION MODEL

The excess electricity generation at one BS will compensate for the deficit at another BS by enabling energy cooperation among the neighboring BSs without sacrificing their own performance. To facilitate energy transfer through the installed physical power lines have some practical constraints e.g. this concept is not plausible for long-haul communication link due to higher installation cost and large resistive power line losses.

The net energy transferred (E_{share}) to the surrounded BS can be computed as

$$E_{share} = E_{sur} - E_{lloss} \tag{31}$$

where E_{lloss} is the energy loss in the resistive conductor in the form of heat during sharing. E_{lloss} is a function of length of the connected power lines and is evaluated over t_r duration in hours as follows [29]

$$E_{lloss} = I^2 R(l) \times t_r = \frac{P_{share}^2 R(l)}{V^2} \times t_r \tag{32}$$

where I is the current passing through the conductor, $R(l)$ is the resistance of the l km conductor length, V is the DC bus-bar voltage (BS operated at 48 V DC). We assume the surplus energy cooperation take place in the DC form for the small geographical region and can be expressed as follows

$$E_{share} = P_{share} \times t_{op} \tag{33}$$

The average energy savings via energy cooperation can be formulated as

$$AES(i, t) = \frac{\sum_{i=1}^{N} E_{share}(t)}{\sum_{i=1}^{N} E_{BS}(t)} \times 100\% \tag{34}$$

where N is the number of transmitting BS, typically 7 BSs for the single-tier configuration and E_{BS} is the total energy demand of i^{th} BS in kWh per year.

Note, the resistance of the connected power cable is 3.276 ohm/km as obtained from the American Wire Gauge (AWG) standard conductor size table [30]. The inter-site distance (ISD) is calculated as $\sqrt{3}$ times of cell radius (i.e. $\sqrt{3}R$). In this paper, we consider 1000m cell radius. Thus, the total resistance over the physical connection between two collocated BSs is 5.67 Ω.

A heuristic technique of energy sharing among the neighboring BSs is developed for maximizing green energy utilization. A BS seek harvested green energy from the surrounded BSs for serving its user without any interruption under insufficiency of input power supply and storage capacity as well. Notably, the green energy sharing take places through the feasible shortest path for minimizing the power loss in the interconnecting resistive transmission line. For energy sharing, the considered BS ranks its neighbors in a descending manner of available green energy storage. This is because a BS intended to share energy from other surrounded BSs having higher green energy stored. There are two different cases for using energy in the BSs, which are discussed as below with respect to the i^{th} BS $\mathcal{B}^i$.

1) CASE I: GENERATION IS HIGHER THAN DEMAND

If $E_{gen}^i(t) \geq E_{BS}^i(t)$, then the i^{th} BS $\mathcal{B}^i$ has sufficient green energy for serving its UEs. Hence, there is no need of green energy sharing from other BSs. The remaining harvested energy in the storage after fulfilling the demand denoted by $G^i(t)$ can be expressed as

$$G^i(t) = E_{gen}^i(t) - E_{BS}^i(t) - B_{loss}^i(t) - C_{loss}^i(t) \tag{35}$$

Therefore, after meeting the demand of time t, available energy in the storage of $\mathcal{B}^i$ for the time slot $(t+1)$ can be written as

$$S^i(t+1) = G^i(t) + E^i_{gen}(t+1) - E^i_{BS}(t+1) \quad (36)$$

where $E^i_{gen}(t+1)$ and $E^i_{BS}(t+1)$ are the generation of combine solar and wind energy, and the total energy demand for time $(t+1)$ respectively.

2) CASE II: GENERATION IS LOWER THAN DEMAND

Energy sharing scenario is arise when there is not adequate input energy for powering the BS $\mathcal{B}^i$ under the condition of $E^i_{gen}(t) < E^i_{BS}(t)$. As a consequence, $\mathcal{B}^i$ seeks for the additional energy from its neighbors, which is the total energy remaining in its own storage. Therefore, the total green energy required to be shared by $\mathcal{B}^i$ at time t can be expressed as

$$E^i_{req}(t) = E^i_{BS}(t) - E^i_{gen}(t) \quad (37)$$

Let the set of sorted BSs in a descending fashion is given by $\mathbb{B}^i = \{\mathcal{B}^{i,1}, \mathcal{B}^{i,2}, \ldots, \mathcal{B}^{i,M}\}$, where M is the number of neighboring BSs of $\mathcal{B}^i$. Now, if the neighboring BS $\mathcal{B}_{i,1}$ has a shareable solar energy $\geq E^i_{req}(t)$, BS $\mathcal{B}^i$ accepts this amount from $\mathcal{B}^{i,1}$ that fulfills its demand. If the shared energy of $\mathcal{B}^{i,1}$ is $< E^i_{req}(t)$, BS $\mathcal{B}^i$ accepts the amount from $\mathcal{B}^{i,1}$ that it can share. For the remaining amount of required energy, BS $\mathcal{B}^i$ seeks to share from $\mathcal{B}^{i,2}$ and continues to the next BSs in $\mathbb{B}^i$. Let $\mathcal{E}^{i,m}_{share}$ be the amount of solar energy shared by $\mathcal{B}^i$ from the neighboring BS $\mathcal{B}^{i,m}$. Then the total energy received by $\mathcal{B}^i$ from the neighboring BSs can be given by

$$\mathcal{E}^i = \sum_{m=1}^{M} \mathcal{E}^{i,m}_{share} \quad (38)$$

However, the energy sharing option is more feasible for hybrid power supplies where the commercial grid supply is not present or not reliable especially in remote BSs. Energy sharing scheme allows to reduce the locally installed RE harvester capacity in neighboring BSs and henceforth, minimize the NPC for the entire cellular system.

IV. COST MODELING

Net present cost (NPC) represents the cost associated for the proposed cellular systems for the life cycle. The total NPC comprises the capital cost (CC) of the system components that pays at the beginning of the project, replacement cost (RC) that occurs during the working period of a component, operation & maintenance cost (OMC) and the salvage value (S) of components. The NPC is computed as follows

$$NPC = \frac{TAC}{CRF} = CC + RC + OMC - S \quad (39)$$

Total annualized cost (TAC) value and capital recovery factor (CRF) is described as follows

$$TAC = TAC_{CC} + TAC_{RC} + TAC_{OMC} \quad (40)$$

$$CRF = \frac{j(1+j)^L}{(1+j)^L - 1} \quad (41)$$

where L is the project lifetime and j is the annual real interest rate.

The salvage value is usually computed at the end of the project lifecycle and applies to components that have longer lifetimes than the project duration.

$$SC = C_{rep}\left(\frac{L_{rem}}{L_{comp}}\right) \quad (42)$$

where C_{rep}, L_{rem}, and L_{comp} are the replacement cost of the component, the remaining lifetime in years, and the lifetime of the component in years respectively.

For the DG enabled hybrid system, fuel cost (FC) also involved in NPC. However, NPC can also be calculated in terms of the associated costs as

$$NPC = CC + RC + OMC + FC - S \quad (43)$$

Levelized cost of energy ($LCOE$) is defined as the ratio of the total annualized cost (TAC) to the annual electricity production (E_{gen}) by the system. $LCOE$ evaluate the financial viability of the project and can be computed as below

$$LCOE = \frac{TAC}{E_{gen}} = \frac{NPC \times CRF}{E_{gen}} \quad (44)$$

V. PROBLEM FORMULATION AND OPTIMIZATION

The hybrid energy system design problem is formulated as an optimization problem with the objective function of minimizing NPC subject to various design and operational constraints. For the hybrid powered cellular system, the design variables include number of wind turbine generator, number of solar PV arrays, number of battery units, and converter size. Several parameter for the system components, such as the operational lifecycle, component efficiency, and associated cost are considered for an efficient performance of the optimization process to formulate the optimal hybrid power system. HOMER decides at each hour to meet electricity demand by cellular RAN infrastructure including losses and provide the backup power also. In each iteration, HOMER calculates the BS load demand to the the input power supply and the optimization step follows all simulations HOMER finds the least cost combination of components that meet BS load while ensuring zero capacity shortage.

$$\text{minimize } NPC \quad (45a)$$
$$\text{subject to } E_{PV} + E_{WT} > E_{BS} \quad (45b)$$
$$E_{PV} + E_{WT} + E_{batt} = E_{BS} + E_{loss} \quad (45c)$$
$$E_{sur} = E_{gen} - E_{BS} - E_{loss} \quad (45d)$$
$$E_{battmin} \leq E_{batt} \leq E_{battmax} \quad (45e)$$

where E_{loss} comprises both battery loss (B_{loss}) and converter loss (B_{loss}) in kWh/yr. The combined energy contribution by solar PV arrays, and wind turbine generator can meet the annual BS demand to ensure power reliability mentioned in (45b). The constraint in (45c) ensures that the annual energy obtained by the renewable energy sources carry the annual BS energy consumption with associated losses. The amount of surplus electricity is preserved for future use during the abnormal condition or shared among neighboring BS due to scarcity of energy is described by the constraint (45d). The constraint (45e) indicates the battery bank storage capacity should not exceed the maximum limit and not reached the below threshold level.

HOMER is the optimization software employed in this study to examine the techno-economic factors optimal hybrid power system that satisfies user-specified constraints with the lowest net present cost (NPC). HOMER decides at each time step to meet the energy requirements at the lower net present cost, subject to the constraint from the dispatch strategy chosen in the simulation. HOMER starts an hourly simulation of every possible configuration, computing the available energy from the solar PV array, sizing of PV capacity, wind turbine generator, number of batteries comparing it to the BS load demand and losses, and deciding to store the surplus renewable energy in times of excess. An integrated renewable powered hybrid scheme must be designed to meet the desired BS load demand at a defined level of security over the expected life time. The system must supply sufficient electricity to both the BS load and the backup power system each hour.

VI. PERFORMANCE ANALYSIS

A. SIMULATION SETUP

In this study, the project duration is assumed to be 15 years that reflects the long-term economic feasibility of the system. The annual capacity shortage is kept 0%. The annual interest rate considered in the simulation setup is 6.75% [31], which affects directly on the overall system cost. Moreover, 10% backup power is reserved to serve the BS load in future, even if the green energy generation suddenly decreases. We assume each BS experiences temporal traffic diversity. Several sets of sizes are considered in the simulation for the different components such as PV module, converter, DG set, battery units to achieve the best solution in the optimization process. In addition, the cost parameters of different elements, duration of average lifecycle of each components, and solar resource profile for particular area are set in HOMER environment. However, on-site installed capacity of wind turbine ($P_{WT} = 1$kW) is kept remains constant throughout this paper. Techno-economic specifications and system constraints of different components are presented in Table 7.

The monthly solar radiation values and clearness index used in this study are obtained using longitude and latitude of Bangladesh. The annual average solar irradiation (γ_{avg}) is 4.59 kWh/m^2/day as seen from Fig. 3. The monthly wind speed data are stringent for remote Patenga area in Bangladesh.

B. RESULT ANALYSIS

In this section, we particularly emphasize on four different prime aspects: (i) optimal system architecture, (ii) technical criteria for PV/WT solutions under different configuration, (iii) energy yield evaluation, and (iv) cost assessment. Thereafter, we compare the techno-economic performance of the proposed system with different power solutions such PV/DG, PV/WT/DG, and standalone PV supply for benchmarking. Relations of network sustainability, cost-effectiveness and greenhouse gas (GHG) emissions with that of various parameters like system bandwidth, transmission power, and daily solar radiation intensities are thoroughly investigated and critically analyzed.

TABLE 7. Simulation setup of hybrid power LTE cellular networks [19].

System Components	Parameters	Value
SPV	Operational lifetime	25 years
	PV derating factor	0.9
	Capital cost	\$1/W
	Replacement cost	\$1/W
	O&M cost/year	\$0.01/W
WT	Size	1 kW
	Hub height	10 m
	Operational lifetime	25 years
	Capital cost	\$1.6/W
	Replacement cost	\$1.6/W
	O&M cost/year	\$0.5/W
Battery	Round trip efficiency	85%
	$B_{SoC_{min}}$	30%
	V_{nom}	6 V
	Q_{nom}	360 Ah
	Capital cost	\$300/unit
	Replacement cost	\$300/unit
	O&M cost/year	\$10
Converter	Efficiency	95%
	Operational lifetime	15 years
	Capital cost	\$0.4/W
	Replacement cost	\$0.4/W
	O&M cost/year	\$0.01/W
Diesel Generator	Efficiency	40%
	Capital cost	\$0.66/W
	Replacement cost	\$0.66/W
	O&M cost	\$0.05/h
	Operational lifetime	25,000h

1) OPTIMAL SYSTEM ARCHITECTURE

The schematic diagrams of an optimal system layout for LTE macro BS under different network settings in HOMER platform are shown in Figs. 11, 12, 13 and 14. Table 8 includes a summary of the optimal size of different components at an average solar radiation with two different transmission power under different system bandwidth for macrocell with RRH. On the other hand, the technical criteria for the optimal

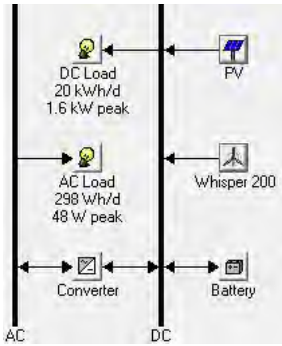

FIGURE 11. Schematic diagram of macro BS with RRH architecture in HOMER for $P_{TX} = 20W$, $\mathcal{BW} = 10$ MHz.

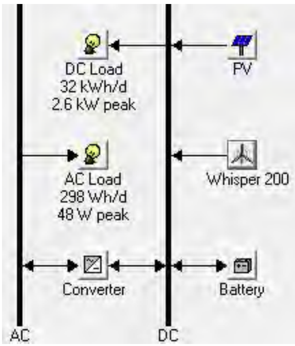

FIGURE 12. Schematic diagram of macro BS with RRH architecture in HOMER for $P_{TX} = 40W$, $\mathcal{BW} = 10$ MHz.

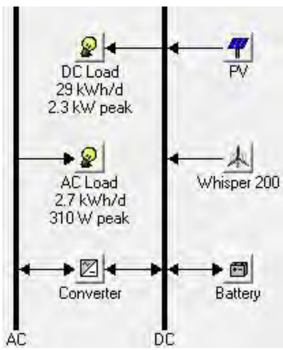

FIGURE 13. Schematic diagram of macro BS without RRH architecture in HOMER for $P_{TX} = 20W$, $\mathcal{BW} = 10$ MHz.

TABLE 8. Optimal system architecture of macrocell with RRH for an average solar radiation varying P_{TX} and $\mathcal{BW}$.

$\mathcal{BW}$(MHz)	PV(kW)		WT(kW)		Battery(units)		Converter(kW)	
	20W	40W	20W	40W	20W	40W	20W	40W
5	1	4	1	1	32	32	0.1	0.1
10	2	5	1	1	32	32	0.1	0.1
15	3	6.5	1	1	32	32	0.1	0.1
20	4	7.5	1	1	32	32	0.1	0.1

system design under the same network settings for macrocell BS without RRH is shown in Table 9.

According to the definition, higher system bandwidth ($\mathcal{BW}$) and transmission power (P_{TX}) uplifts the BS load

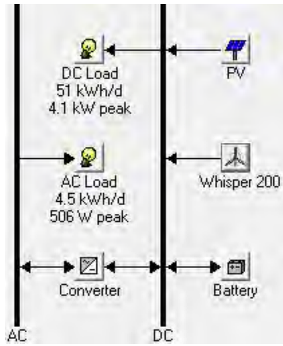

FIGURE 14. Schematic diagram of macro BS without RRH architecture in HOMER for $P_{TX} = 40W$, $\mathcal{BW} = 10$ MHz.

demand and total energy consumption as well. This happens because $\mathcal{BW}$ forces the baseband unit and RF section power to rise whereas, P_{TX} pushed P_{PA} in the upward direction. To deal with the cumbersome BS load demand, a large number of solar PV modules and number of batteries are need to be installed at each BS. It is noteworthy that macro BS without RRH have need of greater solar panels as compared to that of RRH configuration for the particular network settings due to the greater load demand. Consequently, LTE BS without RRH involves more net present cost compared to that of RRH configuration as discussed in the subsequent economic assessment section. Unless otherwise specified, the rest of the results presented in this paper are analyzed considering the proposed macrocell BS with RRH scheme under actual traffic scenario.

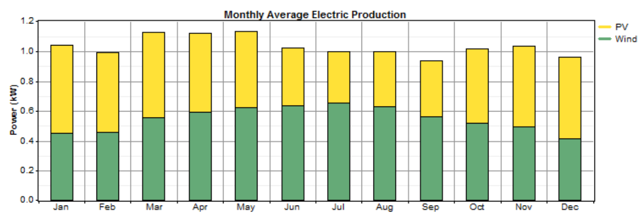

FIGURE 15. Monthly power contribution by hybrid RE sources for $\gamma_{avg} = 4.59$ kWh/m^2/day, $\mathcal{BW} = 10$MHz, and $P_{TX} = 20$W.

Fig. 15 presents the monthly average power production by integrated RE sources for an average solar radiation and average wind speed of 7.48 m/s. The maximum solar PV energy contribution occurred in March and April when the solar radiation is maximum. Meanwhile, the minimum PV energy contribution take place in June and July because of rainy season. However, the wind power is primarily used to feed BS load while the excess energy generation from PV modules are kept reserved for further use. Solar and wind resources often complement each other. This complimentary effect is even greater during seasonal changes as observed from Fig. 15.

Table 10 represents the optimum size of system components for different daily solar radiation intensities under 10 MHz bandwidth using HOMER simulation. As seen,

TABLE 9. Optimal system architecture of macro BS without RRH for γ_{avg} varying P_{TX} and $\mathcal{BW}$.

$\mathcal{BW}$ (MHz)	PV (kW)		WT (kW)		Battery (units)		Converter (kW)	
	20W	40W	20W	40W	20W	40W	20W	40W
5	4	9.5	1	1	32	64	0.2	0.4
10	5	11	1	1	32	64	0.2	0.4
15	6.5	11	1	1	32	128	0.3	0.4
20	8	12	1	1	32	128	0.3	0.4

TABLE 10. Summary of technical criteria for the proposed system varying γ_d and P_{TX} under $\mathcal{BW}$ = 10 MHz.

γ_d (kWh/m^2/day)	PV (kW)		Converter (kW)		Battery (units)		WT (kW)	
	20W	40W	20W	40W	20W	40W	20W	40W
4.0	2	6.5	0.1	0.1	32	32	1	1
4.5	2	5.5	0.1	0.1	32	32	1	1
5.0	1.5	4.5	0.1	0.1	32	32	1	1
5.5	1.5	4	0.1	0.1	32	32	1	1

a higher value of γ_d step down the installed solar array size leading to direct enhancement of PV energy generation to tackle the specified load demand. As stated in (2), the solar energy generation is proportionally varied with γ_d and PV array capacity (C_{PV}). Thus, high solar radiation readily decreases the C_{PV} for the same amount of solar energy production. However, battery bank capacity and converter size remains unchanged as noticed from the Table 10.

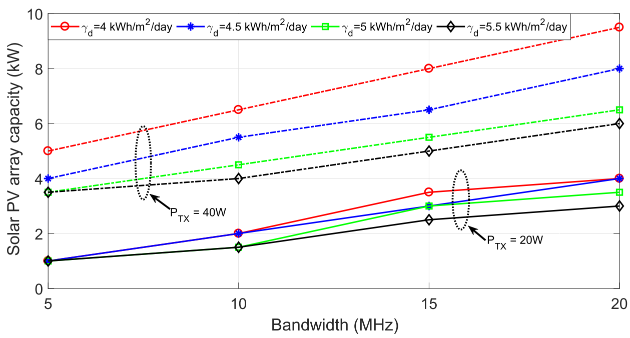

FIGURE 16. PV array capacity vs. bandwidth varying solar radiation (γ_d) and P_{TX} for macro BS with RRH.

Fig. 16 illustrates the installed solar PV array capacity varying P_{TX} and γ_d. All the curves tend to follow upward direction almost in a similar pattern with the increment of bandwidth. The dashed line implies for 40 W transmission power whereas the solid lines in the graph depicted for P_{TX} = 20W throughout the entire paper. As the system bandwidth increases, C_{PV} increases gradually to cope with higher energy consumption. On the other hand, the results for P_{TX} = 20W shows small changes including some slight fluctuations as the BS energy demand not significantly varied with C_{PV}. Besides, solar energy harvester capacity overlaps for 5 MHz and 10 MHz bandwidth due to minor load variation in regard to C_{PV}. As expected, the PV array capacity decreases for the higher solar radiation values. The graph clearly figure out the exact dimension of C_{PV} for the two different P_{TX} under particular bandwidth.

2) ENERGY YIELD EVALUATION

The annual energy contribution of PV array (E_{PV}) and WT (E_{WT}) along with surplus energy (E_{sur}) measurement are discussed based on the optimal system design criteria. In addition, battery bank (BB) autonomy (B_{aut}), BB lifetime (B_{life}), annual throughput (Q_{tp}) have been critically analyzed under various configuration. Moreover, the amount of energy savings (ES) through sharing mechanism via resistive power lines has been thoroughly investigated in the same section.

a: SOLAR PV ARRAY AND WIND TURBINE

According to Table 2 and Table 8, solar PV array consists of 8 and 20 sharp modules for 10 MHz system bandwidth under 20 W and 40 W transmission power respectively. The annual energy contribution of 2 kW solar for an average solar radiation can be calculated using Eq. (2); 2 kW (C_{PV}) × 4.59 kWh/m^2/day (γ_{avg}) × 0.9 (f_{PV}) × 365 days/yr = 3015 kWh. However, dual-axis tacking mode of PV panels increases the total amount of energy by 25% [21] to be 3769 kWh/yr. However, the yearly solar energy generation for different network configuration can be computed in the similar way. On the other hand, HOMER calculates the annual wind energy production for 1 kW WT is 4797 kWh which remains constant over the entire paper.

Fig. 17 demonstrates the annual PV production varying P_{TX} and γ_d. Likewise Fig. 16, all the curves follow a similar pattern to reach maximum value to meet with up trending energy demand. With the increase of bandwidth, E_{PV} of the proposed network models substantially improves, which is mainly due to the increasing number of installed PV panels. Moreover, higher PV energy generation is found for the lower value of daily solar radiation due to the larger C_{PV} as evident from the figure. Once again, the separation of E_{PV} curves are very insignificant for P_{TX} = 20W.

b: SURPLUS ELECTRICITY

HOMER calculates the battery loss (B_{loss}) and converter loss (C_{loss}) of 177 kWh and 6 kWh respectively for P_{TX} = 20W, γ_{avg} = 4.59 kWh/m^2/day, $\mathcal{BW}$ = 10 MHz

TABLE 11. Energy contribution and surplus electricity in kWh for P_{TX} = 20W, γ_{avg} = 4.59 kWh/m^2/day.

$\mathcal{BW}$(MHz)	E_{PV}	E_{WT}	E_{BS}	B_{loss}	C_{loss}	E_{sur}
5	1884	4797	6048	90	6	537
10	3769	4797	7520	177	6	863
15	5654	4797	9000	410	6	1136
20	7539	4797	10474	566	6	1390

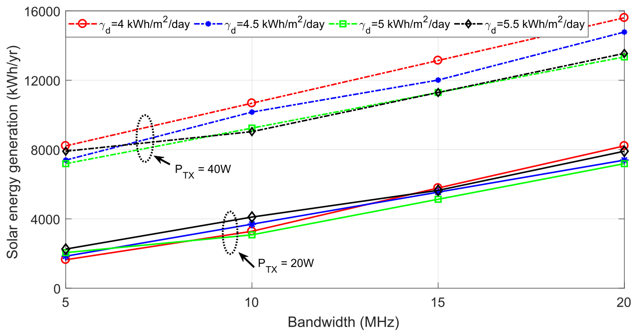

FIGURE 17. PV energy generation with $\mathcal{BW}$ varying γ_d and P_{TX}.

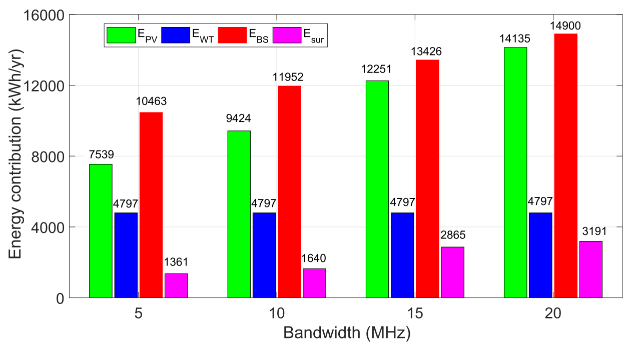

FIGURE 18. Annual energy contribution and excess electricity for P_{TX} = 40W, γ_{avg} = 4.59 kWh/m^2/day.

network settings. Annual surplus electricity (E_{sur}) can be computed using Eq. (30); 3768 kWh (E_{PV}) + 4797 kWh (E_{WT}) - 7520 kWh (E_{BS}) - 177 kWh (B_{loss}) - 6 kWh (C_{loss}) = 862 kWh/yr. The annual excess electricity generation for other network configurations can be found in a similar way. Table 11 illustrates the statistical analysis of yearly energy contribution by RE sources including surplus electricity for various system bandwidth. A comprehensive comparison of annual energy provision of hybrid supplies together with E_{sur} is shown in Fig. 18 under P_{TX} = 40W and γ_{avg}. The excess electricity generation is moved upward direction with the higher solar energy generation as seen from the Fig. 18 and Table 11. The greater value of E_{sur} implies the better system reliability as the proposed system could independently meet the BS load demand without any support from external non-RE sources like DG supply. A detail comparison of surplus energy generation under distinctive network settings is depicted in Fig. 19. The excess energy curves are found

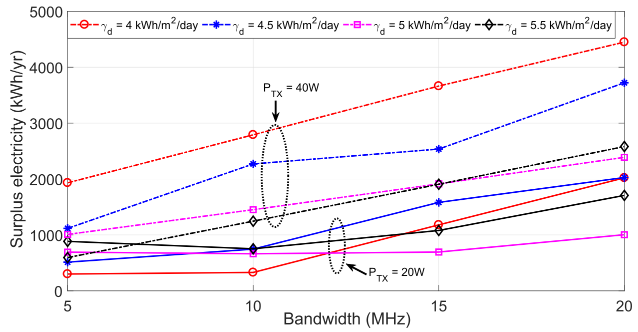

FIGURE 19. Surplus electricity vs. $\mathcal{BW}$ varying γ_d and P_{TX}.

to reach their peak values with the increment of system bandwidth for both transmission power. E_{sur} for the least solar radiation value follows an opposite trend up to 10 MHz bandwidth under two different P_{TX}. This is happens due to the variation of PV module capacity since the solar radiation values has the direct impact on PV array capacity and solar generation as well. The simulation results imply the same results as explained in Fig. 18.

c: ENERGY SAVING VIA COOPERATION MECHANISM

Energy cooperation technique among neighboring BSs allows maximum utilization of locally generated RE and helps in curtailing associated energy cost. The feasibility and the mathematical model of energy sharing mechanism is described in section III-J. According to the definition, shared electricity can be derived by subtracting resistive line loss from the excess electricity generation. The amount of transferred energy between surrounded BS for P_{TX} = 20W is illustrated in Fig. 20. Under the proposed network model, the BSs would share electricity among themselves in a possible shortest path to minimize line loss occurred in the power lines after fulfilling its own demand. However, the line current flows through an overhead power lines is 2.05 ampere and the annual line loss incurred about 208 kWh in accordance with Eq. (32). Therefore, the energy saving using overhead power cable for a single BS is about 8.72%.

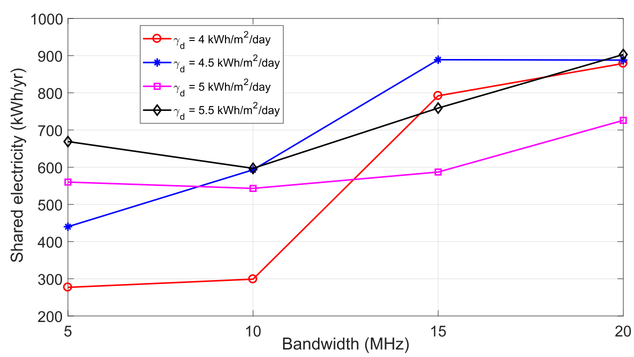

FIGURE 20. Shared electricity among neighboring BS with bandwidth for P_{TX} = 20W varying γ_d.

TABLE 12. Annual energy savings in percentage for P_{TX} = 20W, γ_{avg} = 4.59 kWh/m^2/day.

$\mathcal{BW}$ (MHz)	$E_{sur}(kWh)$	$I(Amp)$	$E_{lloss}(kWh)$	$E_{sh}(kWh)$	$ES(\%)$
5	537	1.27	80.8	456	7.55
10	863	2.05	208	355	8.72
15	1136	2.7	361	775	8.62
20	1390	3.3	539	851	8.13

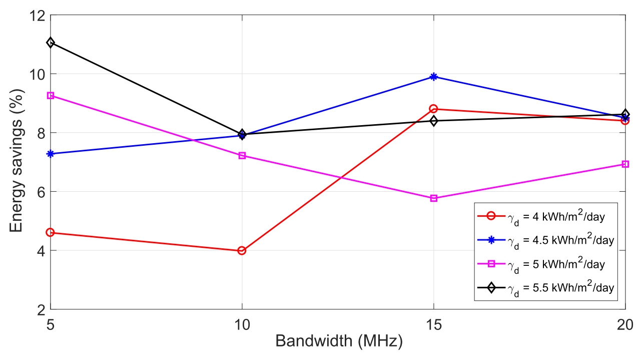

FIGURE 21. Energy savings via energy cooperation mechanism for P_{TX} = 20W varying γ_d.

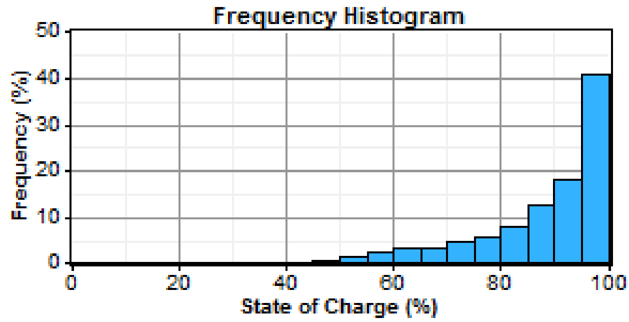

FIGURE 22. Annual frequency histogram of SoC for $P_{TX} = 20W$, $\mathcal{BW}$ = 10 MHz, γ_{avg} = 4.59 kWh/m^2/day.

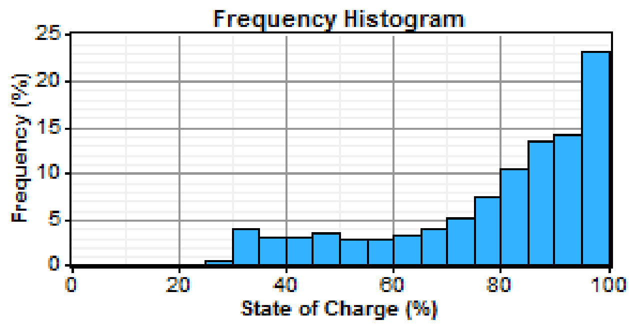

FIGURE 23. Annual frequency histogram of SoC for $P_{TX} = 40W$, $\mathcal{BW}$ = 10 MHz, γ_{avg} = 4.59 kWh/m^2/day.

Table 12 manifest the details computation of energy saving varying $\mathcal{BW}$. However, the saving will be enhanced if the energy sharing take place from the multiple surrounded BSs. Therefore, the promising option of intelligent energy sharing mechanism can significantly minimize installed PV capacity and also downsize the energy costs correspondingly. The percentage of energy saving between two collocated BSs is presented in Fig. 21 for P_{TX} = 20W varying γ_d and exhibits the similar pattern like Fig. 20. The figure depict that the proposed model keeps its optimistic nature achieving energy saving for higher value of γ_d. This implies that the energy savings is dependent predominantly on the solar energy generation.

d: BATTERY BANK

The total number of battery units are required for the all RRH configuration is 32; connected 8 in series and 4 in parallel to be compatible with the 48 V DC bus bar for the LTE macro BS. The battery bank autonomously support the BS about 57.2 hours, which is calculated using Eq. (17) for $P_{TX} = 20W$, $\mathcal{BW}$ = 10MHz, and γ_{avg} configuration; (N_{batt} = 32 × V_{nom} = 6V × Q_{nom} = 360 Ah × B_{DoD} = 0.7 × 24hr)/daily BS load, L_{BS} = 20.3 kWh. Battery bank autonomy varies with BS load consumption and $\mathcal{BW}$ as well for the particular battery model regardless the solar radiation exposure. The frequency histogram shown in Fig. 23 demonstrates that the battery bank is in a minimal SoC for approximately 1% of the year and high SoC for approximately 23% of the year. The result signifies that additional set of battery units are required within project duration.

A detailed comparison of battery bank autonomy (B_{aut}), lifetime (B_{life}), and annual throughput (Q_{tp}) are illustrated in Figs. 24, 25 and 26 respectively. A higher value of B_{aut} and B_{life} are preferable for reliable and cost-effective cellular architecture to carry the BS load for a prolong period of time. A better performance of B_{life} inherently reduces the replacement cost in turns of overall NPC. B_{aut} gradually decreases with the system bandwidth as the daily BS load consumption

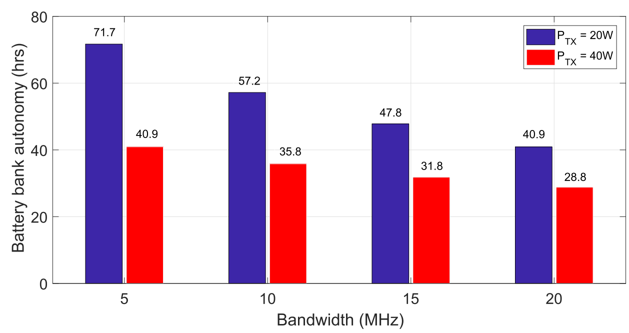

FIGURE 24. Variation of battery bank autonmoy with bandwidth for different P_{TX} under γ_{avg}.

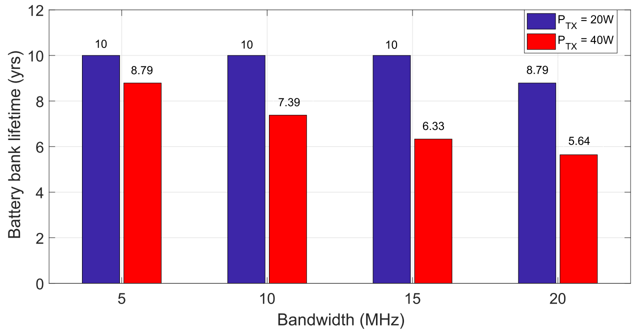

FIGURE 25. Battery bank lifetime vs. $\mathcal{BW}$ for γ_{avg} varying P_{TX}.

increases correspondingly. The results for $P_{TX} = 40$W shows pessimistic nature due to the higher BS load demand. The graph implies that the LTE BS operating under 20W transmission power offer superior autonomy hours during RE sources failure. However, B_{aut} performance of the proposed system is found significantly better for smaller load consumption as illustrated in figure. For instance, the battery bank carry the BS load demand independently about 71.7 hours (almost 3 days) without any support from an external retailers under 5 MHz system bandwidth. It can be safely concluded that B_{aut} ensure a higher level of reliability with zero outage.

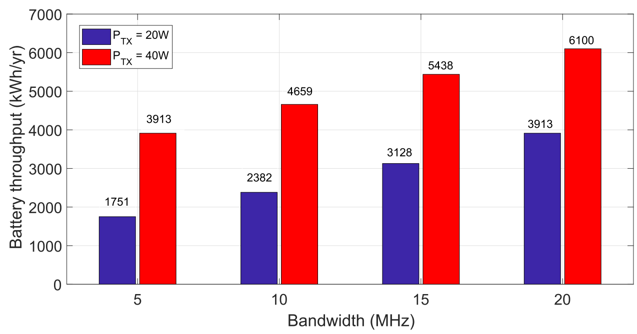

FIGURE 26. Throughput comparison of storage device for γ_{avg} varying P_{TX}.

Impact of yearly battery throughput (Q_{tp}) on the B_{life} is depicted in Fig. 26. As seen, B_{life} demonstrate the opposite trend of Q_{tp} according to Eq. (18) and the simulation results signify the same results as seen from Fig. 25 and Fig. 26. Battery lifetime refers to the number of times a battery can fully charged and discharged before reaching the end of their operational life. Energy throughput defines the amount of energy in a battery bank can be expected to store and deliver over its lifetime. A gradual decrement of B_{life} is found for the higher system bandwidth under $P_{TX} = 40$W, whereas B_{life} is stand fixed under all the cases for $P_{TX} = 43$ dBm except 20 MHz bandwidth. However, B_{life} is a crucial factor as it directly involves to the replacement cost over the project duration. Therefore, from the view point of C_{PV}, B_{aut}, B_{life} and NPC, macrocell operated at 20W offer better economic solution as compared to 46 dBm transmission power.

The subsequent results presented in the cost assessment section gives the clear view of the individual associated cost involved with the proposed scheme varying system parameters.

3) COST ASSESSMENT

The breakdown of the gross capital cost (CC), O&M cost (OMC), replacement cost (RC), salvage value (S), and net present cost (NPC) incurred within the project duration are calculated using data from Table 7. The capital cost is paid once at the beginning of the project based on the installed component size of the system. Besides, the bulk of the replacement costs goes to the components having short cycle duration relative to considered project duration. Salvage value is an estimated amount of an asset that is expected to be received at the end of project duration. For instance, the life-cycle for the assumed poly-crystalline sharp solar module is 25 years, whereas 15 years project lifetime is considered over the entire paper. This means that solar array get back salvage for the remaining 10 years.

TABLE 13. Cost analysis breakdown of different components for γ_{avg}, P_{TX} = 20W, and $\mathcal{BW}$ = 10 MHz under macro BS with RRH configuration.

Components	CC	RC	OMC	S	NPC
PV	2,000	0	185	300	
WT	600	0	46	0	
Battery	9,600	4,996	2,961	1,802	**18,335**
Converter	40	0	9	0	
Total cost	12,240	4,996	3,202	2,102	

Table 13 summarizes the individual cost analysis breakdown of different components for the proposed hybrid powered cellular system. Based on the cost analysis breakdown, the nominal cash flow for γ_{avg} and $P_{TX} = 40$W is shown in Fig. 27. Capital cost of renewable energy products is considerably high as observed from the figure. OMC is involved periodically at every year. In addition, battery replacement constitute a major portion of NPC.

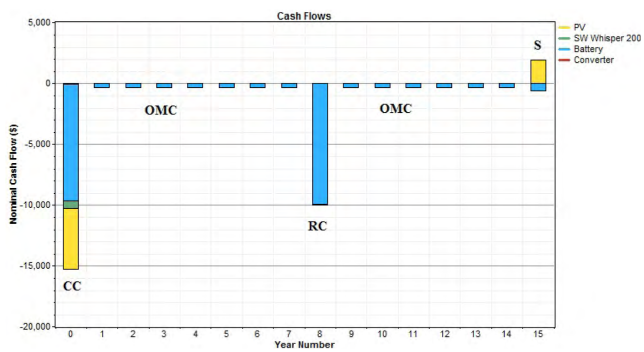

FIGURE 27. Cash flow summary of the hybrid PV/WT power system for γ_{avg}, P_{TX} = 40W and $\mathcal{BW}$ = 10 MHz.

Table 14 presents the NPC comparison for macrocell without RRH scheme under $P_{TX} = 20$W and γ_{avg}. The integration of RRH with macrocell substantially minimize NPC

TABLE 14. Summary of the economic criteria for γ_{avg}, P_{TX} = 20W under macro BS without RRH configuration.

$\mathcal{BW}$ (MHz)	CC ($)	RC ($)	OMC ($)	S ($)	NPC ($)
5	13,780	5,308	3,350	1,773	20,665
10	15,280	5,883	3,489	748	23,903
15	16,820	10,414	3,637	3,432	27,439
20	18,160	11,195	3,831	2,571	31,314

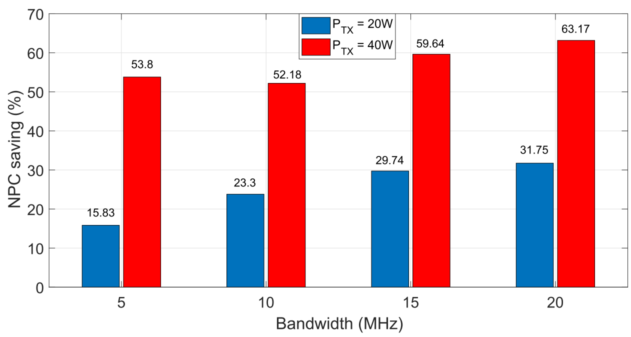

FIGURE 28. Percentage of NPC savings between macrocell with RRH and macrocell without RRH for γ_{avg} varying P_{TX}.

about 23.3% as evident from the Table 13 and Table 14 for $\mathcal{BW}$ = 10 MHz. The benefits of RRH integration in LTE BS on NPC savings is clearly demonstrated in Fig. 28 for different transmission power. Macrocell with RRH attained superior NPC savings about 31.75% for P_{TX} = 20W and $\mathcal{BW}$ = 20 MHz case, while apparently positive impact for P_{TX} = 40W is also observed. To the end, macro BS with RRH scheme outperforms other system in terms of energy yield and *NPC* for the same level of QoS.

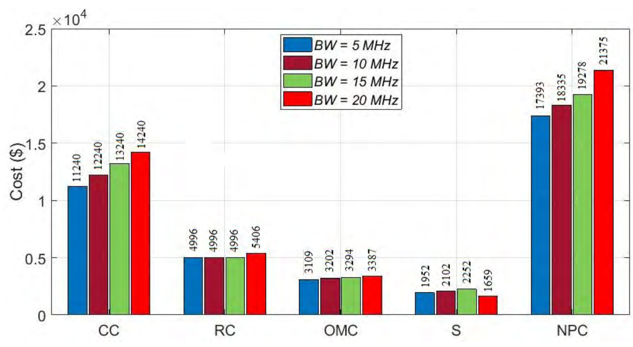

FIGURE 29. Comparison of cost analysis varying bandwidth for γ_{avg} = 4.59 kWh/m^2/day, P_{TX} = 20W.

Fig. 29 and Fig. 30 illustrates the summary of individual cost analysis for the entire cellular system varying bandwidth and solar radiation intensities respectively. As expected, large $\mathcal{BW}$ give rise to high NPC owing to the larger solar installed capacity. In contrast, high solar radiation intensity push downward the NPC for the particular P_{TX} as explain beforehand.

From the aforementioned analysis, the NPC curve follows up trending manner to reach their maximum value with the

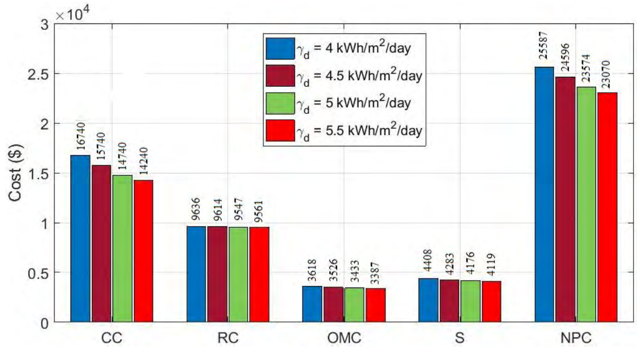

FIGURE 30. Comparison of cost analysis varying γ_d for $\mathcal{BW}$ = 10 MHz, P_{TX} = 40W.

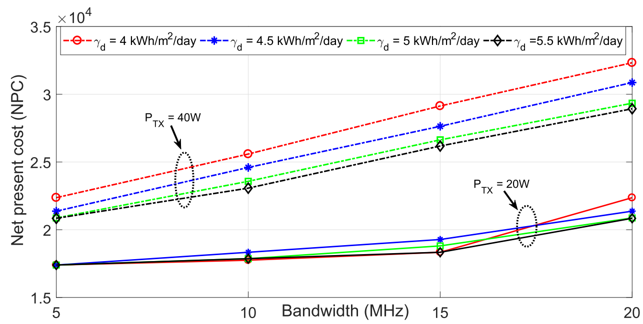

FIGURE 31. NPC comparison varying γ_d and P_{TX}.

increment of system bandwidth as clearly seen in Fig. 31. On the other hand, lower solar irradiation and large P_{TX} forces *NPC* to upward direction. In addition, The *NPC* gap is more apparent for 40W transmission power mode as previously explained of Fig. 16.

A detail quantitative comparison of the levelized cost of electricity (*LCOE*) with system bandwidth is demonstrated in Fig 32. *LCOE* evaluates the per unit cost of electricity for the specified network configuration. A gradual decrement of *LCOE* has been found for the higher BW under P_{TX} = 20W. On the other hand, *LCOE* variation is very insignificant for 40W case as both the *NPC* and E_{gen} maintain almost in a proportional relationship. Also, an improved *LCOE* performance is noticed for higher system bandwidth.

Impact of daily solar radiation intensity (γ_d) in *LCOE* is exhibited in Fig. 33 for P_{TX} = 20W. All the curve follows a continuous decreasing manner with the system bandwidth following the Fig. 32. A higher value of γ_d attains superior *LCOE* performance for any specified BW as evident from the figure. LTE BS operated at the higher bandwidth require greater RE harvester capacity to be installed leading an increasing amount of net present cost despite the potential advantage of lower *LCOE*.

4) COMPARISON ANALYSIS

The optimal design of the proposed system must satisfy the BS load demand including associated losses. The size of

TABLE 15. Techno-economic comparison of PV/DG hybrid power supply system for γ_{avg} and P_{TX} = 20W.

$\mathcal{BW}$(MHz)	PV(kW)	DG(kW)	Battery(unit)	Converter(kW)	NPC($)	LCOE($/kWh)	B_{life}(yr)	F_c(L)	t_{op}(hr)	CO_2(kg)
5	4	1	32	0.3	21,398	0.393	9.68	94	550	252
10	5	1	32	0.3	24,834	0.365	7.85	143	837	383
15	5.5	1	32	0.3	28,026	0.349	6.73	212	1248	568
20	7	1	32	0.3	31,680	0.338	5.83	223	1315	598

TABLE 16. Techno-economic comparison of PV/WT/DG hybrid power supply system for γ_{avg} and P_{TX} = 20W.

$\mathcal{BW}$(MHz)	PV(kW)	WT(kW)	DG(kW)	Battery(units)	Conv.(kW)	NPC($)	LCOE($/kWh)	B_{life}(yr)	F_c(L)	t_{op}(hr)	CO_2(kg)
5	1	1	1	32	0.1	17,809	0.326	10	0	0	0
10	2	1	1	32	0.4	19,273	0.281	10	81	405	217
15	2.5	1	1	32	0.1	20,207	0.246	10	88	474	236
20	4	1	1	32	0.2	22,418	0.234	8.83	55	353	147

TABLE 17. Techno-economic comparison of standalone PV power supply system for γ_{avg} and P_{TX} = 20W.

$\mathcal{BW}$ (MHz)	PV (kW)	Battery(units)	Converter (kW)	NPC ($)	LCOE ($/kWh)	B_{life} (yr)
5	4	32	0.1	19,844	0.372	9.61
10	5.5	32	0.1	23,276	0.347	7.81
15	7	32	0.1	26,860	0.336	6.61
20	9	32	0.1	30,870	0.329	5.73

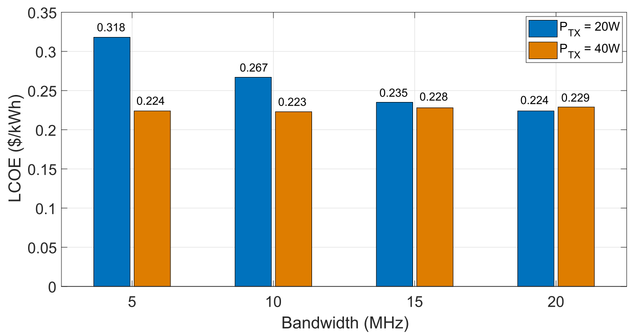

FIGURE 32. LCOE vs. $\mathcal{BW}$ for different P_{TX} under γ_{avg}.

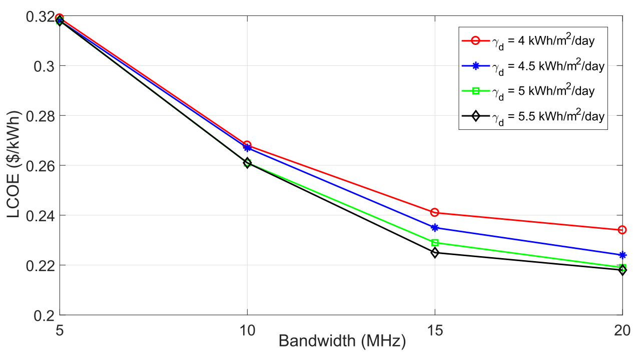

FIGURE 33. Comparison of LCOE vs. $\mathcal{BW}$ for P_{TX} = 20W.

PV/WT hybrid system is directly related to the BS energy consumption as it varies with the system bandwidth. In this section, the techno-economic comparison of the proposed PV/WT enabled cellular system with that of different combination such as PV/DG, PV/WT/DG scheme, and standalone PV system is carried out for benchmarking. The comparative analysis of the PV/DG, PV/WT/DG and only PV powered cellular networks are summarized in Table 15, 15 and 15 respectively for the same network settings. The optimum size of individual components along with cost evaluation are presented in each table. A considerable amount of carbon footprints is involved in PV/DG and PV/WT/DG configurations due to the fuel consumption. The *NPC* and *LCOE* manifest in PV/DG system are considerably high over the proposed method. Moreover, the performance of battery bank lifetime has been degraded for the higher load consumption as apparent from the Table. On the other hand, *NPC*, *LCOE*, and B_{life} values for PV/WT/DG scheme are almost near to the proposed system but generate GHG emissions. Therefore, both PV/DG and PV/WT/DG system have become less preferable over PV/WT arrangement. It can be safely inferred that hybrid PV/WT powered LTE cellular networks can fully eliminate carbon footprints over the mentioned two hybrid supply schemes. Furthermore, a large number of PV modules are needed to be installed to cater desired BS demand under standalone PV supply system leading a remarkable enhancement of *NPC* as well as *LCOE*. Moreover, B_{life} performance over the year is not satisfactory as compared to the proposed framework. Therefore, the proposed PV/WT system ensures a greater level of eco-sustainability and has been proved as a feasible option for the envisioned off-grid green cellular networks.

A comparison of *NPC* saving of the proposed model with other schemes is demonstrated in Fig. 34. The network is simulated for average solar irradiation with P_{TX} = 20W. From the figure, a clear distinction of NPC savings is observed among different power supply schemes implementing on the macrocell with RRH networks. NPC performance of the standalone PV system lies in between in between PV/WT/DG and PV/DG power supply solutions as it involves lower *NPC*. It is further found that PV/DG and standalone PV system shows inferior *NPC* performance with the system $\mathcal{BW}$ and leaving a little influence on the percentage of NPC savings. On the other hand, PV/WT/DG system has shown small variations of NPC saving. For example, the proposed system attain 5%, 22%, and 26% *NPC* savings compared to PV/WT/DG, standalone PV and PV/DG system respectively at a specific 10 MHz bandwidth. From the analysis of this figure, once again the PV/WT system has been recognized as a suitable option for powering LTE BS from the point of view of *NPC* reduction.

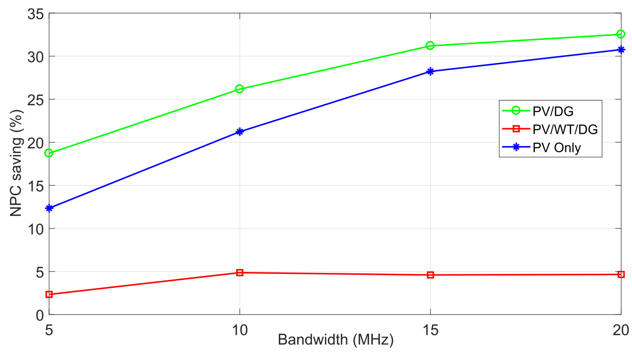

FIGURE 34. Comparison of NPC saving among different power supply scheme for γ_{avg} and P_{TX} = 20W.

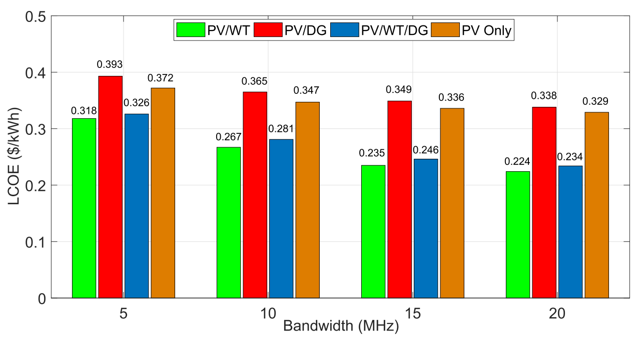

FIGURE 35. LCOE Comparison among different power supply scheme for γ_{avg} and P_{TX} = 20W.

Finally, an extensive comparison of *LCOE* among different power supply scheme along with the proposed system is illustrated in Fig. 35. It is clearly identified that the hybrid PV/WT power cellular system has achieved superior *LCOE* performance over all the designated schemes under all cases. To the end, the proposed PV/WT system perform a lot better than other power supply schemes. Therefore, it can be safely inferred that solar-wind hybrid technology with energy sharing technique is a preferable choice for long-term energy efficient and cost effective solution in a remote cellular base stations.

VII. CONCLUSION

In this paper, we have investigated the feasibility and effectiveness of hybrid renewable energy sources integration into remotely located off-grid LTE macrocell BS endeavoring to minimize both NPC and greenhouse gas emissions. A surplus green energy cooperation strategy has also been proposed for achieving energy efficient cellular networks. In powering a BS with integrated RE sources along with energy cooperation mechanism can effectively use in hill areas, remote islands has been proved as a preferred choice over pollution intensive DG or grid supplies. In light of this, a sensitivity analysis including optimal system architecture, energy savings, and energy-cost analysis have been carried out in the particular study area using HOMER software package. For benchmarking, the proposed system is then compared with the different combination of possible power supply schemes. System performance has been evaluated varying different parameters, such as bandwidth, transmission power and daily solar radiation exposure. Simulation results have shown that the proposed system could meet the required energy demand independently with guaranteed reliability. The battery bank can easily feed the BS load autonomously for a prolonged period of time without any external support, which is a sufficient time to fix hybrid system malfunctions. In addition, energy sharing mechanism has been figured out more effective for improving energy savings and also curtail the energy costs correspondingly. Moreover, a substantial impact of solar radiation exposure, transmission power and bandwidth have been found during techno-economic assessment. Furthermore, the proposed system contribute zero carbon emissions compared to that of other power supply solutions and ensure better eco-sustainability through green engineering solutions. In summary, the PV/WT enabled hybrid energy system has been identified as an attractive long-term economical and energy-efficient solution for the envisioned green cellular networks. The degree of system performance is predominantly dependent on the network scenarios and the availability of ambient green energy sources.

REFERENCES

[1] M. J. Farooq, H. Ghazzai, A. Kadri, H. ElSawy, and M. Alouini, "A hybrid energy sharing framework for green cellular networks," *IEEE Trans. Commun.*, vol. 65, no. 2, pp. 918–934, Feb. 2017.

[2] A. Jahid, A. B. Shams, and M. F. Hossain, "Dynamic point selection CoMP enabled hybrid powered green cellular networks," *Comput. Electr. Eng.*, pp. 1–15, Mar. 2018.

[3] K. Kanwal, G. A. Safdar, M. Ur-Rehman, and X. Yang, "Energy management in LTE networks," *IEEE Access*, vol. 5, pp. 4264–4284, 2017.

[4] A. M. Aris and B. Shabani, "Sustainable power supply solutions for off-grid base stations," *Energies*, vol. 8, no. 10, pp. 10904–10941, Sep. 2015.

[5] M. A. Safwat, "Framework for multi-operator collaboration for green communication," *IEEE Access*, vol. 6, pp. 850–865, Nov. 2018.

[6] M. Ismail, W. Zhuang, E. Serpedin, and K. Qaraqe, "A survey on green mobile networking: From the perspectives of network operators and mobile users," *IEEE Commun. Surveys Tuts.*, vol. 17, no. 3, pp. 1535–1556, 3rd Quart., 2014.

[7] A. Jahid, A. B. Shams, and M. F. Hossain, "Green energy driven cellular networks with JT CoMP technique," *Phys. Commun.*, vol. 28, no. 1, pp. 58–68, Jun. 2018.

[8] S. Dutta, T. Geiger, and B. Lanvin, "The global information technology report: ICTs for inclusive growth," World Economic Forum, Geneva, Switzerland, Tech. Rep., 2015.
[9] A. Abrol and R. K. Jha, "Power optimization in 5G networks: A step towards GrEEn communication," *IEEE Access*, vol. 4, pp. 1355–1374, 2016.
[10] M. H. Alsharif, R. Nordin, and M. Ismail, "Energy optimisation of hybrid off-grid system for remote telecommunication base station deployment in Malaysia," *EURASIP J. Wireless Commun. Netw.*, vol. 2015, no. 1, p. 64, Dec. 2015.
[11] P. Gandotra, R. K. Jha, and S. Jain, "Green communication in next generation cellular networks: A survey," *IEEE Access*, vol. 5, pp. 11727–11758, 2017.
[12] V. Chamola and B. Sikdar, "Solar powered cellular base stations: Current scenario, issues and proposed solutions," *IEEE Commun. Mag.*, vol. 54, no. 5, pp. 108–114, May 2016.
[13] H. A. H. Hassan, A. Pelov, and L. Nuaymi, "Integrating cellular networks, smart grid, and renewable energy: Analysis, architecture, and challenges," *IEEE Access*, vol. 3, pp. 2755–2770, 2015.
[14] Y.-K. Chia, S. Sun, and R. Zhang, "Energy cooperation in cellular networks with renewable powered base stations," *IEEE Trans. Wireless Commun.*, vol. 13, no. 12, pp. 6996–7010, Dec. 2014.
[15] H. Ghazzai, E. Yaacoub, A. Kadri, H. Yanikomeroglu, and M. Alouini, "Next-generation environment-aware cellular networks: Modern green techniques and implementation challenges," *IEEE Access*, vol. 4, pp. 5010–5029, Sep. 2016.
[16] Y. Zhang, M. Meo, R. Gerboni, and M. A. Marsan, "Minimum cost solar power systems for LTE macro base stations," *Comput. Netw.*, vol. 112, no. 1, pp. 12–23, Jan. 2017.
[17] M. H. Alsharif, "Optimization design and economic analysis of energy management strategy based on photovoltaic/energy storage for heterogeneous cellular networks using the HOMER model," *Solar Energy*, vol. 147, no. 1, pp. 133–150, May 2017.
[18] J. Gong, J. S. Thompson, S. Zhou, and Z. Niu, "Base station sleeping and resource allocation in renewable energy powered cellular networks," *IEEE Trans. Commun.*, vol. 62, no. 11, pp. 3801–3813, Nov. 2014.
[19] M. H. Alsharif and J. Kim, "Hybrid off-grid SPV/WTG power system for remote cellular base stations towards green and sustainable cellular networks in South Korea," *Energies*, vol. 10, no. 1, p. 9, Dec. 2016.
[20] Y. Chiang and W. Liao, "Green multicell cooperation in heterogeneous networks with hybrid energy sources," *IEEE Trans. Wireless Commun.*, vol. 15, no. 12, pp. 7911–7925, Dec. 2016.
[21] A. Jahid and M. S. Hossain, "Energy-cost aware hybrid power system for off-grid base stations under green cellular networks," in *Proc. IEEE Int. Conf. Electr. Inf. Commun. Technol. (EICT)*, Khulna, Bangladesh, Dec. 2017, pp. 1–6.
[22] A. Jahid, A. S. Ahmad, and M. F. Hossain, "Energy efficient BS Cooperation in DPS CoMP based cellular networks with hybrid power supply," in *Proc. IEEE Int. Conf. Comput. Inf. Technol. (ICCIT)*, Dhaka, Bangladesh, Dec. 2016, pp. 93–98.
[23] *System Advisor Model (SAM)*. Accessed: Jan. 17, 2018. [Online]. Available: https://sam.nrel.gov/
[24] P. O. Oviroh and T.-C. Jen, "The energy cost analysis of hybrid systems and diesel generators in powering selected base transceiver station locations in Nigeria," *Energies*, vol. 11, no. 3, p. 687, Mar. 2018.
[25] A. Chauhan and R. P. Saini, "A review on integrated renewable energy system based power generation for stand-alone applications: Configurations, storage options, sizing methodologies and control," *Renew. Sustain. Energy Rev.*, vol. 38, no. 1, pp. 99–120, Oct. 2014.
[26] M. S. Hossain, A. Jahid, and D. M. F. Rahman, "Quantifying potential of hybrid PV/WT power supplies for off-grid LTE base station," in *Proc. IEEE Int. Conf. Comput., Commun., Chem., Mater. Electron. Eng. (IC4ME2)*, Rajshahi, Bangladesh, Feb. 2018, pp. 1–5.
[27] A. Jahid and M. S. Hossain, "Feasibility analysis of solar powered base stations for sustainable heterogeneous networks," in *Proc. IEEE Region 10 Humanitarian Technol. Conf.*, Dhaka, Bangladesh, Dec. 2017, pp. 686–690.
[28] H. Holtkamp, G. Auer, V. Giannini, and H. Haas, "A parameterized base station power model," *IEEE Commun. Lett.*, vol. 17, no. 11, pp. 2033–2035, Nov. 2013.
[29] A. Jahid and S. Hossain, "Intelligent energy cooperation framework for green cellular base stations," in *Proc. IEEE Int. Conf. Comput., Commun., Chem., Mater. Electron. Eng. (IC4ME2)*, Rajshahi, Bangladesh, Feb. 2018, pp. 1–6.
[30] Solaris Technology Industry Inc. *American Conductor Wire Size*. Accessed: Mar. 27, 2018. [Online]. Available: https://www.solarisshop.com/content/AmericanWireGaugeConductorSizeTable.pdf
[31] *Bangladesh Bank Monetary Policy*. Accessed: Feb. 6, 2018. [Online]. Available: https://tradingeconomics.com/country-list/interest-rate?continent=asia

ABU JAHID (S'17) received the bachelor's and M.Sc. degrees in electrical engineering from the Military Institute of Science and Technology, Dhaka, Bangladesh, in 2010 and 2018, respectively. From 2010 to 2012, he was with Huawei Technologies, where he was researched on radio network planning and optimization. Since 2016, he has been serving as an Assistant Professor with the Department of Electrical, Electronic and Communication Engineering, Military Institute of Science and Technology. He has co-authored numerous articles in leading journals and IEEE conference proceedings. His research interests include the design and modeling of energy efficient green cellular networks.

MD. KAMRUL HASAN MONJU received the B.Sc. degree in electrical engineering from the Bangladesh University of Business and Technology, Dhaka, Bangladesh, in 2017. His current research interests include wireless communications and renewable energy.

MD. EMRAN HOSSAIN received the bachelor's degree in electrical and electronic engineering from the Bangladesh University of Business and Technology in 2017. His current research interests include green communications and optimization.

MD. FARHAD HOSSAIN (S'10–M'14) received the B.Sc. and M.Sc. degrees in electrical and electronic engineering (EEE) from the Bangladesh University of Engineering and Technology, Dhaka, Bangladesh, in 2003 and 2005, respectively, and the Ph.D. degree in electrical and information engineering from The University of Sydney, Australia, in 2014. He is currently an Associate Professor with the Department of EEE, Bangladesh University of Engineering and Technology. He is also an Electrical and Electronic Engineering Consultant. He has published over 50 refereed articles in highly prestigious journals and conference proceedings. His research interests include green cellular networks, underwater communications, smart grid communications, sensor networks, network architectures, and protocols designs. He was a recipient of the best paper award in three international conferences and the Student Travel Grant from the IEEE Global Communications Conference, Anaheim, CA, USA, in 2012. He has been serving as a TPC member and a reviewer in many international journals and conferences.